STRUCTURAL AND METAMORPHIC INVESTIGATION OF THE CATHEDRAL ROCK – DREW HILL AREA, OLARY DOMAIN, SOUTH AUSTRALIA.

Jonathan Clark (B.Sc.)

Department of Geology and Geophysics
University of Adelaide

This thesis is submitted as a partial fulfilment for the Honours Degree of a Bachelor of Science

November 1999

Australian National Grid Reference
(SI 54-2) 1:250 000

ABSTRACT

The Cathedral Rock – Drew Hill area represents a typical Proterozoic high-grade gneiss terrain, and provides an excellent basis for the study of the structural and metamorphic geology in early earth history. Rocks from this are comprised of Willyama Supergroup metasediments, which have been subjected to polydeformation.

The highly strained nature of the area has been attributed to three deformations. These have been superimposed into a single structure, the Cathedral Rock synform, which represents a second-generation fold that refolds the F_1 axial surface.

Pervasive deformation with a northwest transport direction firstly resulted in the formation of a thin-skinned duplex terrain. Crustal thickening in the middle to lower crust led to the reactivation of basement normal faults in a reverse sense. Further compression, led to more intense folding and thrusting associated with the later part of the Olarian Orogeny.

Strain analysis has shown that the region of greatest strain occurs between the Cathedral Rock and Drew Hill shear zones. Cross section restoration showed that this area has undergone approximately 65% shortening. Further analysis showed that strain fluctuated across the area and was affected by the competence of different lithologies and the degree of recrystallisation.

Contents

LIST OF PLATES, TABLES AND FIGURES

ACKNOWLEDGMENTS

There are many people who deserve mention for their help in the work put into this thesis and if.. First of all I would like to thank my supervisor, Dr Pat James, for his help and support both before and during the past year. Thankyou for your help, both out in the field and at home base.

A special thankyou must go to Colin Conor and the Department of Primary Industries and Resources (PIRSA), for the opportunity to do this project, and the associated logistics and funding. Thanks must also go to Mike Szpunar from PIRSA for his help in the field.

The departmental and technical staff of the Department of Geology and Geophysics must also be thanked for their continual help and support throughout the year. These include Gerald Buttfield, Wayne Mussared, Sherry Proferes , Yvonne Philp and Sondra Gould.

I must also thank my fellow structural students, Anthony Ried, Matt Bruce, Simon Constable and Ashley Taylor, especially the later two (my field) partners for many fun-filled days in and out of the field.

I must thank Ron Baxter for allowing us to do our fieldwork on his sheep station, and I hope we kept the stables nice and shippy. I hope the sheep that found its way into the fire place is OK. I must also thank our neighbour from Old Boolcoomata, Malcolm, who suffered the extreme *cold* with us (personal joke).

Last but definitely not least, I must thank Alice Sandford for her moral support and motivation throughout the year. I know I was a handful but I promise I'll make it up to you.

Chapter 1 Introduction

Proterozoic high-grade gneiss terrains provide an excellent basis for the study of structural and metamorphic geology in early earth history. The Cathedral Rock – Drew hill area provides good outcrop of such rocks. The high strain nature of the study area makes it ideal for strain analysis.

1.1. Review of Structural and Strain Analysis in High-Grade Gneiss Terrains

Geological investigation in high-grade Precambrian gneiss terrains typically consist of outcrop analysis, assessment of metamorphic conditions and the determination of the three dimensional distribution of rock units, structures and minerals (Passchier *et. al.,* 1990). Structural data is obtained using conventional mapping techniques as described by Hobbs *et. al.,* (1976) and McClay (1987) where applicable. Form surface mapping at the 1:10000 scale involves the structural analysis of individual fabric elements including layering, foliations and fold axial surfaces.

Localised areas of intense shear strain known as shear zones (Ramsay and Graham, 1970) produce characteristic fabrics. Shear zones represent the ductile equivalent of brittle fault zones. More intensely strained rocks are commonly located in the centre of shear zones (Tourigny and Tremlay, 1997) and it is here that mylonitic and ultra-mylonitic fabrics are formed. The degree of strain is responsible for the formation of different structures and fabrics within shear zones. Structures that form in shear zones include mylonitic fabrics, S-C fabrics, asymmetric porphyroclasts, sheath folding, boudinage structures and extensional crenulation cleavages (ECC's) (Hanmer and Passchier, 1991).

The deformation producing the strain in the rocks is achieved by a large number of processes that affect every grain (Passchier and Trouw, 1998). For this reason, accurate quantification of strain is obtainable only at the grain scale. The more broad scale quantification of strain can be determined using structural elements on the mapped scale; for example progressive deformation will affect angles between planes. One method for determining such bulk strain is to measure the angle between layering and schistosity (Ramsey and Huber 1987) over outcrop scale of major regions of folding and shearing. The use of grain scale microstructures

is another method for determining the deformation processes in operation (Passchier and Trouw, 1998). The foliations that develop in rocks can be used to determine such things as strain and metamorphic conditions.

Fold shapes in high-grade gneiss terrains also indicate degree of strain. Modifications to original fold styles can be used to quantify the degree of flattening (Ramsey and Huber, 1987). Folds also form as a result of shearing and if there is an irregularity in a foliation plane, shear stresses will cause sheath folding (Cobbold and Quinquis, 1979).

This study attempts to describe strain and fabric development within shear zones, in order to define the relative importance of deformation with respect to the regional tectonic framework.

1.2. Location of Study Area

The study area is near Bimbowrie station approximately 120km WSW of Broken Hill, NSW (Figure 1.1). The Olary Domain (OD) contains surface exposures of basement rocks of the Willyama Supergroup. These basement rocks preserve a complex structural and metamorphic history typical of Proterozoic gneiss terrains.

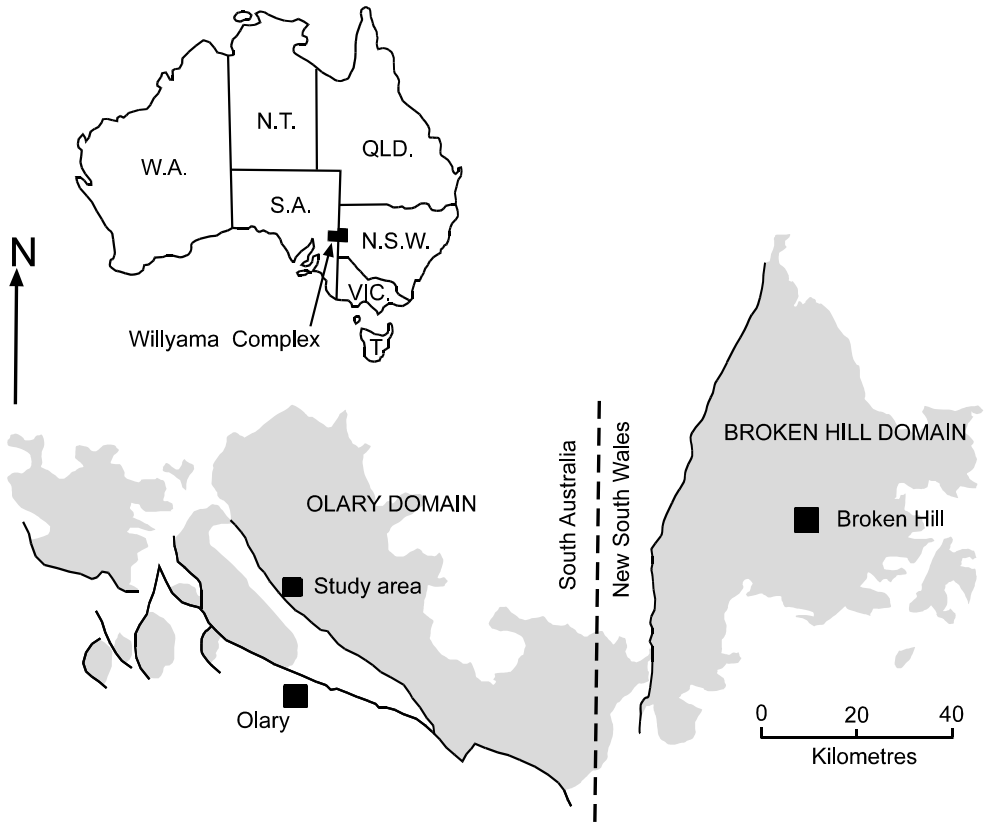

Figure 1.1. Location of the study area within the Olary Domain.

The regional geology and tectonic setting of the Olary Domain is well studied, Ashley *et. al.* (1996), Bierlien (1995), Flint and Parker (1993) and Clarke *et. al,* (1986). The Old Boolcoomata area has been the focus of several detailed studies (Wiltshire 1975, Archibald 1980). However an improved understanding of the structural and metamorphic evolution on the mapped scale may have implications for the broader regional geological history.

The Cathedral-Rock Drew Hill area is within the highly strained limb of a major refolded syncline (Cathedral Rock synform). This structure is well exposed and is the basis for this study.

1.3. Aims and Research methods

Primary Industries and Resources SA (PIRSA) provided the basic questions for this study. The primary objectives are to investigate the style of deformation and geometry of the structures in the Cathedral Rock – Drew Hill area. This investigation is then used to determine the tectonic setting and structural evolution of the Willyama supergroup in the OD.

The investigation involved both a fieldwork and laboratory analysis component. Detailed structural and lithological mapping at a 1:10000 scale and cross section construction was undertaken in an attempt to analyse the geometrical relationship of the highly deformed rocks. This analysis included the investigation of structures concentrating on the outcrop scale where detailed field sketches were produced using grid-mapping methods outlined by James and Clark (1993). Structural data were analysed using *StereoNett*© a stereoplotting program. Samples were collected and their mineral assemblages and microstructures analysed in an attempt to define the deformation style and metamorphic conditions of specific events. The geometric analysis of folds and faults in the area was then used to semi-quantify the degree of strain associated with these particular structures.

As many of the rocks had been subject to partial melting and alteration which affects large areas within the OD an understanding of the timing and nature of these melt products with respect to deformation events was used in an attempt to determine the broad geological history of the area. Qualitative analysis of the style of these events and their relationship to the regional geological history were used to attempt to explain their timing and nature.

Chapter 2 Regional Geology

2.1. Regional Geology and Tectonic Setting

The Cathedral Rock-Mount Mulga area includes basement rocks of the Willyama supergroup. The Willyama, Mount Painter and Mount Babbage inliers are all part of the Proterozoic Curnamona Province. The Curnamona Province extends from the northern Flinders ranges in the northwest to south of Broken Hill in the southeast. The Willyama Supergroup comprises a sequence of late Palaeoproterozoic meta-sedimentary and meta-volcanic rocks, local metamorphosed intrusives, and early Mesoproterozoic volcanic and sedimentary rocks and granitoid intrusives. The Willyama inlier is comprised of the Olary and Broken Hill domains. Work done on both the geology and the mineral deposits of these areas has indicated that there are distinct similarities between them.

Stevens *et al.* (1990) correlated the Willyama Supergroup of the Broken Hill domain with the Olary Domain. Two major litho-stratigraphic schemes have been proposed for the area (Stevens *et al.,* 1990 and Ashley *et al.,* 1996), including the earlier 'lower Albite', 'middle schist', and 'upper Albite' terminology. A more widely used, later terminology is represented in figure 2.1.

Willis *et al.* (1983) interpreted the Willyama supergroup to be part of a failed Palaeoproterozoic rift system, which was subsequently deformed and metamorphosed. The Olary Domain is thought to represent the rift margin shelf setting. Evidence derived from local volcanism, immature terrigenous and volcanoclastic sediments would seem to indicate deposition in a lacustrine to marine setting. The Broken Hill domain (BHD) is thought to represent the central part of the former rift system. The two domains are separated by the Mundi-Mundi Fault and a major gravity and magnetic discontinuity, continuing to the southwest.

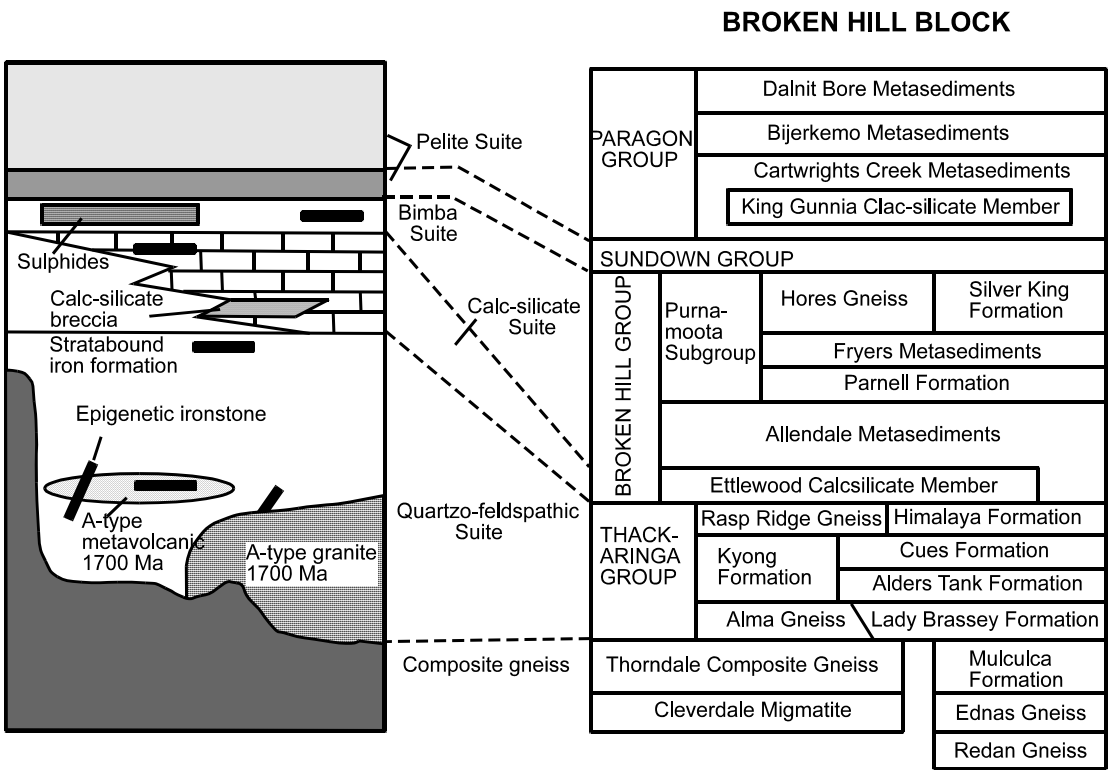

Figure 2.1. Interpreted correlation of the Willyama sequence between the Olary and Broken Hill domains. After Ashley *et al.* (1998) and Clarke *et al.,* (1986)

2.2. Stratigraphy

The lithological sequence to be used herein is the scheme proposed by Clarke *et al.* (1986). Five main lithologies are described below including the 'Composite Gneiss', 'Quartzofeldspathic', 'Calcsilicate', 'Bimba' and 'Pelite' Suites (Fig. 2.1).

Composite Gneiss Suite

The 'Composite Gneiss Suite' is interpreted as being the basal unit of the Willyama complex (Clarke *et al*., 1986). It is characterised by coarse grained quartz-feldspar-biotite ± sillimanite ± garnet gneisses. These are primarily of meta-sedimentary origin (Ashley *et al*., 1998).

Quartzofeldspathic Suite

The 'Quartzofeldspathic suite' contains the lower and upper Albite units, and the Middle schist formation. The "Lower Albite" unit contains numerous large bodies of leucocratic gneiss. The rocks of this unit constitute foliated to massive, thickly layered albite - quartz (± K-feldspar ± biotite ± muscovite ± magnetite ± pyrite) supracrustals. The Upper Albite unit commonly

consists of well laminated, fine-grained, albite - quartz (± K-feldspar ± biotite ± magnetite ± calc-silicates) rock. The Middle Schist consists of psammopelitic schist, minor psammite, quartzofeldspathic gneiss and composite gneiss. This unit commonly occurs between the lower and upper albite units. The lower part of the 'Quartzofeldspathic suite' has experienced a much higher degree of anatectic melting, with the formation of migmatites and banded migmatitic and massive leucocratic granitiods.

Calcsilicate Suite

The 'Calcsilicate suite' is thought to be diachronous with respect to the "Upper Albite" unit of the 'Quartzofeldspathic' suite. It grades from calc-silicate bearing albite into calc-silicate type rocks in its upper part (Bierlien, 1995). It is characterised by thickly to thinly laminated beds, which are correlated with stratabound calc-silicate matrix breccias (eg. Cathedral Rock). The relationships are consistent with the deposition of the calc-silicates which are thought to have been deposited in an oxidising, sabkha or lacustrine/playa environment with local hot spring activity (Cook and Ashley, 1992: Cook, 1993).

Bimba Suite

The 'Bimba Suite' forms a thin (<50m, typically much thinner in the OD) laterally continuous unit of quartz-biotite-albite±muscovite±sillimanite metasiltsones which are inter-layered with marble, albitic chert and calc-silicate gneiss. It is also associated with stratiform iron-dominant sulphides, which have oxidised to form gossanous outcrops. In areas of high strain, such as the "Cathedral Rock" synform, the Bimba Suite is identified by ferruginous and gossanous float.

The 'Bimba Suite' is a transitional unit between the underlying interpreted evaporitic sediments and the overlying deep-water marine sediments. Flint and Parker (1993) suggested a shallow marine environment as its depositional setting.

Pelite Suite

Outcrops of the Pelite suite are dominated by pelitic and psammopelitic schist (biotite + muscovite + quartz ±alumino-silicates ± garnet ± tourmaline) and locally grade into thin psammites in the upper part of the sequence. Locally the best way of recognising the Pelite Suite is by the presence of aluminosilicate porphyroclasts.

Flint and Parker (1993) proposed that the original sediments were deposited in a deep marine setting, undergoing subsidence. The sediments consist of interbedded turbiditic muds and silts.

2.3. Structural History

Investigations by Wiltshire (1975), Berry *et al*. (1978), Armstrong (1980), Clarke *et al*. (1986; 1987) and Flint and Parker (1993) have resulted in the recognition of five phases of deformation in the OD. The first three phases termed OD_1, OD_2 and OD_3 were developed during the Olarian Orogeny (1600-1500 Ma), The last two deformations termed DD_1 and DD_2 were attributed to the Delamerian Orogeny and affect both the Willyama and the Adelaidean cover sequences.

OD_1 is characterised by mesoscopic to macroscopic, tight to isoclinal recumbent OF_1 folds. The axial surface of the OF_1 folds (OS_1) is defined by the preferred dimensional orientation of micaceous minerals. The distinction between OS_1 and the sub-parallel limbs of the OF_2 folds is difficult. The OD_3 structures are generally tight to open, mesoscopic to macroscopic, upright to steeply inclined folds. These have clearly defined axial plane fabrics. The Delamerian deformational events (DD_4 and DD_5) typically produce N-NNW trending fold axes. Later E-NE trending fold axes are recognised in the Adelaidean cover sequence (Flint and Parker, 1993).

There is local overprinting of the Willyama Complex rocks by Delamerian deformation (Clarke *et al*., 1986) with reactivation of Olarian shear zones. The timing of this event is synchronous with DD_2 (Ashley *et al*., 1998).

2.4. Metamorphic History

Based on the mineral assemblages in metapelitic rocks, Clarke *et al*. (1987) have divided the OD into 3 metamorphic zones (Fig. 2.2). The Olarian Orogeny is characterised by an anticlockwise P-T-t path (Fig 2.3). This path was determined using the timing relationships obtained from the aluminosilicate polymorphs associated synchronously with deformational events (Flint and Parker, 1993).

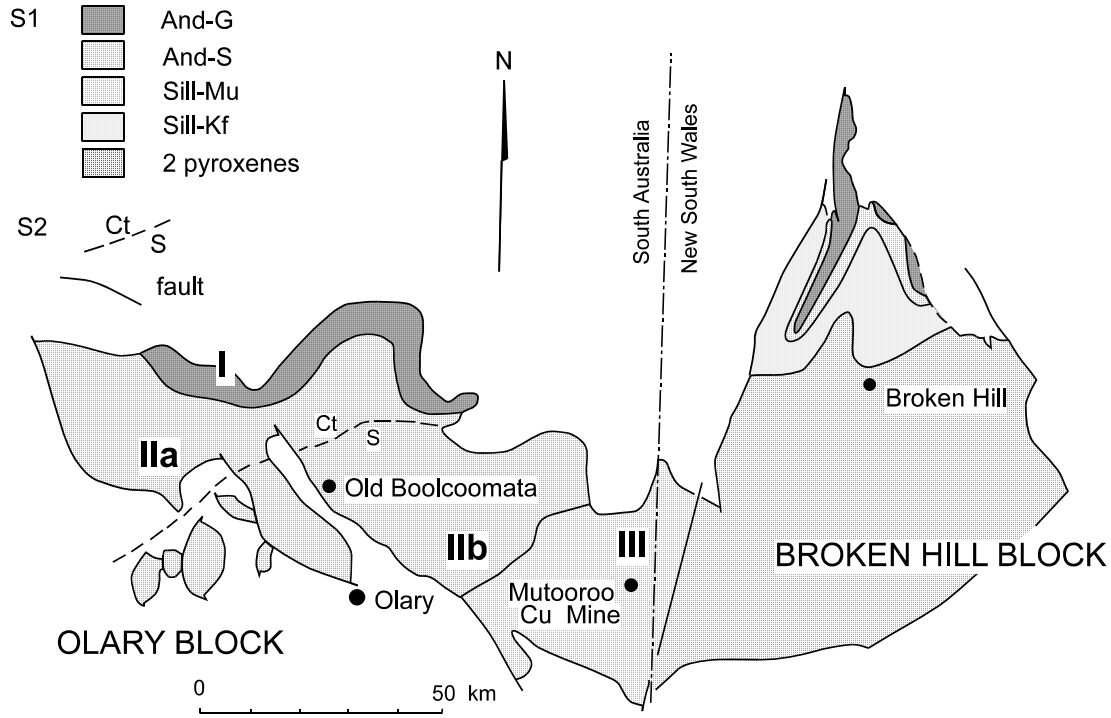

Figure 2.2 Distribution of metamorphic zones determined by aluminosilicate assemblages in metapelites through the Olary and Broken Hill Domains. After Clarke *et al*. (1987). And – Andalusite; G – Garnet; S - Staurolite; Mu - Muscovite; Kf - Pottasium Feldspar: Ct - Cordierite

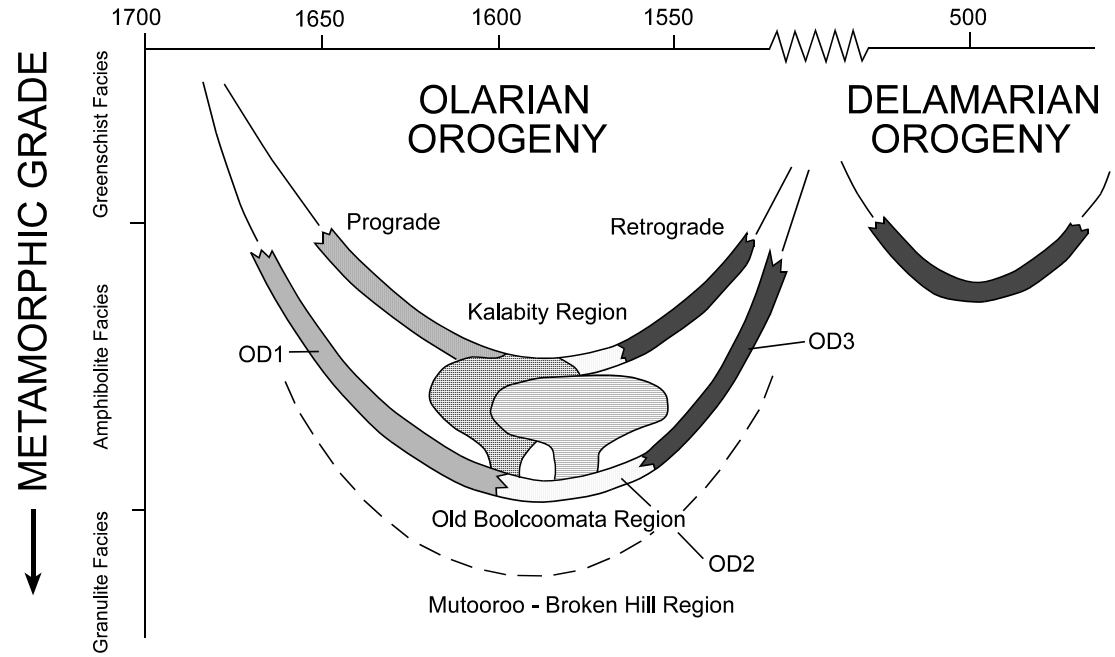

Figure 2.3 Timing and metamorphic grade of the Olarian and Delamerian deformational events (Flint and Parker, 1993).

2.5. Alteration

Many of the rocks in the OD have been affected by hydrothermal alteration (Ashley *et al*., 1998). On a regional scale sodium and iron alteration is dominant. Sodium alteration is manifest in certain rock types as albite and iron as magnetite, haematite and pyrite.

Chapter 3 Lithological Variation

The following chapter describes the mapped lithologies and their distribution across the area. Both field and petrological descriptions are provided for each lithology. Figure 3.1 shows the stratigraphic positions of these units with respect to each other.

3.1. Metasediments

'Migmatised Quartzofeldspathic Gneiss'

Migmatised quartzofeldspathic gneisses are the oldest rocks to outcrop in the mapped area. With respect to other units, they are more intensely deformed (plate 1b) and contain a larger proportion of migmatites. Mineralogy consists of quartz, feldspar (albite) magnetite and minor muscovite and biotite. The more schistose layers consist of quartz, feldspar, and a much larger proportion of muscovite and biotite.

'Iron Rich Schist'

A thin layer (1-5m) thick of an *iron rich pelite* outcrops within *the migmatised quartzofeldspathic gneiss*. This unit is slightly more resistant than other schistose layers within the migmatised quartzofeldspathic gneiss. In outcrop is has a distinct rusty colour. It seems that this unit has been affected by oxidation. Magnetite and pyrite crystals are found in the more highly strained portions of the rock. The mineralogy consists of quartz, muscovite, feldspar, magnetite and a fine grained matrix comprising mineral grains and cataclastic flows. High strain fabrics wrap around larger mineral grains.

'Layered Quartzofeldspathic Gneisses and Schists'

This unit is lithologically very similar to the *layered gneiss* apart from having a much larger proportion of migmatite. Albite rich quartzofeldspathic gneisses are interbedded with more schistose layers. The quartzofeldspathic layers consist of quartz, feldspar, biotite, muscovite and magnetite. Quartz grains exhibit undulose extinction, and the local formation of sub-grains is prominent.

The more schistose layers represent psammitic and pelitic beds. These beds consist of fine to medium grained biotite, muscovite, quartz and plagioclase. Biotite and muscovite define the foliation.

Figure 3.1.

GEOLOGY OF DREW HILL - CATHEDRAL ROCK AREA, OLD BOOLCAMATA, OLARY.

GN MN

MAGNETIC DECLINATION 8°

MAP LOCATION

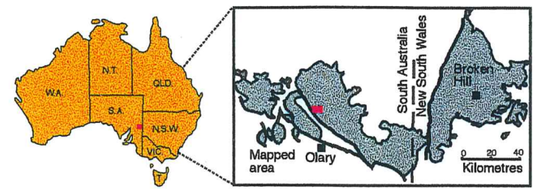

Drafted by Jonathan Clark B.sc
Department of Geology and Geophysics
University of Adelaide
November 1999.

Australian mapping Grid S1-54-2

RAVEN HILL MINE

RAVEN HILL SOUTH MINE

SCALE - 1 : 10 000

100 0 100 200 300 400 500 METRES

LEGEND

- Creek
- Track
- Geological Boundary
- Geological Boundary (Inferred)
- Fault/Shear
- Quarry/Mine
- Antiform
- Overturned synform
- Synform
- Overturned antiform
- Bedding (So)
- Schistosity (S1)
- Younging

LITHOLOGY

- Alluvium
- Retrograde Shear Zone
- Pegmatite
- Amphibolite
- Granite
- Granitiod Dyke
- Foliated Granitiod Gneiss

WILLYAMA SUPERGROUP

- Platy schist
- Laminated schist Ironstone and gossan
- Layered Quartz, Biotite, Feldspar rock
- Quartz rich mylonite with 'quartz-eyes'
- Albite altered rock
- Brecciated calc albite
- Laminated feldspar rock
- Psammopelitic gneisses and muscovite schists
- Albitic Quartzite
- Layered Gneiss
- Porphyroblastic Muscovite Schist
- Iron Rich Quartzite
- White Quartz Albitite
- Coarse Grained Quartzite with large Quartz Clasts
- Foliated Quartz, Feldspar, Magnetite Rock
- Iron rich blue Quartzite
- Layered Quartzofeldspathic Gneisses and Schists
- Iron Rich Schist
- Migmatised Quartzofeldspathic Gneisses

'Iron Altered Blue Quartzite'

The boundary between this unit and the overlying *foliated quartz, feldspar, magnetite rock* in some places appears gradational. Weathered outcrops of this lithology have a dusty iron stained surface and exhibit spheroidal weathering. Fractures within the quartzite are also iron stained. A fresh surface appears as massive medium grained recrystallised quartz and minor plagioclase with a distinct blue/grey colour. Within this matrix there are larger grains of quartz and plagioclase, which may represent remnent phenocrysts. This may suggest a volcanic origin also.

'Foliated Quartz, Feldspar, Magnetite Rock'

This lithology forms a distinct buff yellow weathered outcrop. In outcrop it contains distinct 'quartz eyes' and laminations defined by pyrite and magnetite. The composition of this rock consists primarily of equant interlocked grains of quartz and feldspar. Under thin section, the textures and mineralogy observed would imply a volcanic origin. Dynamic recrystallisation has obliterated most of the original fabric (S_1). Quartz ribbons and the preferential alignment of mineral grains indicate an overprinting deformation (OD$_2$ or OD$_3$).

'Coarse grained Quartz Clastic'

This unit is very similar in mineralogy to the white quartz albite overlying it, however it contains a larger proportion of quartz occurring both in the matrix and as large clasts ranging from 3 to 7mm in diameter.

'White Quartz Albite'

Generally similar to the *Albitic Quartzite*, the *white quartz albite* unit, outcrops as a massive white to buff, medium grained rock. A weak layering is defined by the alignment of quartz, albite, magnetite and biotite grains. The boundary between this unit and the underlying coarse-grained quartz clastic is hard to distinguish and may be some gradational feature. This unit contains quartz eyes up to 5mm in length, possibly suggesting it is volcanogenic. This unit is typically 10-30m thick.

The past four units are interpreted as having a volcanic orogin as found by Paul Ashley and his honours students (Ashley *et al.,* 1998)

'Iron rich Quartzite'

Outcrops of the *Iron rich quartzite* form ridge tops of maroon coloured resistant, spheroidally weathered quartzite. It consists mostly of quartz and plagioclase with minor biotite, magnetite and pyrite, which define some remanent layering, considered to be bedding. This unit forms a layer approximately 25m thick. It appears to be largely recrystallised.

'Porphroblastic Muscovite Schist'

This unit consists of remnant interbedded psammitic and pelitic layers (S_0) which have been overgrown by muscovite porphyroblasts which have been crenulated by a later deformation. The muscovite porphyroblasts overgrow previous mineral assemblages and appear to have formed from a retrograde event. The mineralogy of this unit consists of muscovite, quartz, feldspar (albite), and minor biotite and magnetite.

'Layered Gneiss'

The *layered gneiss* consists of interbedded layers of psammopelites and albite rich rock. This unit is largely migmatised, with melt segregations forming within the more pelitic layers.

'Albitic Quartzite'

This unit consists of a hard resistant, white albite rich quartzite. It reaches a maximum thickness of 35m on the southern limb of the Cathedral rock synform but is correlated with a much thicker unit (>200m) on the northern limb. It forms a distinct ridge top on the southern limb.

'Psammopelitic gneisses and muscovite schists'

The *interbedded psammopelitic gneisses and muscovite schists* form an inhomogeneous unit 20-80m thick on the southern limb of the Cathedral Rock synform, and reaches a thickness of 120m on the northern limb. The mineralogy of this unit consists of quartz, muscovite, biotite, feldspar ± sillimanite, andalusite and magnetite. Distinct layers of crenulated muscovite schists are interbedded with more albitic psammopelites, which are migmatised. The base of this layer is marked by an albitic quartzite.

'Laminated Feldspar Rock'

Outcrops of this unit vary significantly in appearance laterally. This is largely due to the varying abundance of albite content (sodium alteration) and the degree of strain. Fine-grained quartz and albite with minor biotite, muscovite and magnetite dominate the mineralogy of this

unit. This unit is largely recrystallised. Quartz exhibits undulose extinction, and larger grains have broken down into equi-dimensional sub grains.

On the southern limb of the Cathedral Rock synform it reaches thicknesses of 200m and up to 400m on the northern limb. Mylonitic bands of up to 10m thick occur in areas of high strain. These mylonites typically consist of highly strained quartz grains, albite and minor muscovite (<1%). They contain thin layers of slightly larger grains, which possibly represents some remnant lithological variation (S_0). S-C fabrics and extensional crenulation cleavages (ECC's) are abundant.

Layers of calc-silicate occur throughout this unit. The calc-silicates consist of laminated to thin-bedded rocks, consisting of epidote, actinolite, magnetite and minor biotite and muscovite. Calc-silicate breccias also occur in this unit, such as those forming the Cathedral Rock landform. Albite alteration seems to have preferentially occurred in different layers.

'Quartz rich mylonite with 'Quartz eyes"'

In outcrop this unit appears as a resistant buff/white fine-grained rock with distinct quartz 'eyes'. In thin section it consists of <0.1mm grains of mostly quartz (>90%) and minor K-feldspar (Albite), biotite and magnetite. It occurs as a thin (<5m) layer, which lenses in and out throughout the laminated feldspar unit. This unit appears highly strained with individual grains aligned perpendicular to the principal strain direction (~N-S).

'Layered Quartz, Biotite, Feldspar Rock'

This unit consists of psammopelites dominated by thick quartz rich psammites with thin interbedded biotite rich schists. The mineralogy of this unit consists of quartz, feldspar, biotite, muscovite, garnet, sillimanite, magnetite and tourmaline. An early fabric is typically sub-parallel to S_0 and is defined by muscovite and biotite. Crenulations are relatively common (sample A1121-21). The crenulations are defined by the rotation of previously aligned muscovite crystals. The thickness of this unit is typically 20-80m.

'Laminated schist, Ironstone and Gossan'

The lithologies in this unit are consistent with those of the Bimba Formation (Appendix B). This unit outcrops discontinuously around the Cathedral Rock synform. In the Cathedral Rock-Drew Hill region it reaches a maximum thickness of 2m but is typically 0.5 m thick.

Outcrop of the Bimba Formation typically consists of buff yellow to rusty brown gossans and ironstone's. Laterally the lithology varies between this and laminated schists.

The rock typically consists of quartz, plagioclase (albite), muscovite, biotite and magnetite/pyrite. It is the weathering of the sulphides such as pyrite that leads to the formation of gossans.

'Platy schist'

This unit is the youngest metasediment outcropping within the mapped area. It occurs in the hinge of the Cathedral rock synform. The mineralogy of this unit consists of muscovite, quartz, sillimanite, sericite, feldspar ± magnetite, garnet and graphite. Chlorite is seen occasionally (A1121-Q, see chapter 6). In the more quartz rich layers quartz ribbons have formed with main fabric and undulose extinction is common with the formation of sub-grains within quartz grains. In hand specimen a distinct S-C fabric has formed. In thin section garnet porphyroblasts have been rotated with the S_2 fabric wrapping around them (see chapter 6).

Due to the highly transposed nature of the area, and the high metamorphic grades, sedimentary features are rare. This makes any detailed analysis of the sedimentary characteristics of rock units difficult.

3.2. Intrusives

' Amphibolite'

There are several outcrops of amphibolite in the Cathedral Rock – Drew Hill area. The most prominent are those which outcrop in the Drew Hill Granitiod Gneiss. The Drew Hill Amphibolite's (DHA) are present in the form of dykes that have intruded the Drew Hill Granite (DHG), (Constable, 1999 and Taylor, 1999). Mineralogy of these amphibolites consist of hornblende (45%), plagioclase (30%), quartz (15%), opaque minerals (5-10%) ± biotite, epidote and rutile (Constable, 1999). The grain size ranges from fine to medium and they exhibit minor foliation development.

Other minor amphibolites occur in the area. These are usually highly strained and occur in more albitic units.

'Drew Hill Granite'

The DHG is a large granitiod gneiss that outcrops in the southern region of the mapped area. The DHG is coarse grained and mineralogically homogeneous. The mineral composition of the DHG consists of quartz (45%), plagioclase (40%), biotite (30%), muscovite (5%) opaque minerals (5%) ± hornblende, zircon and sphene.

In hand specimen one foliation is distinct, and is defined by the alignment of biotite.

'Granitiod Dyke'

A granitiod dyke approximately 10m thick appears to have intruded into *the migmatised quartzofeldspathic gneiss*. It is mineralogically very similar to the DHG, but is much coarser grained.

'Pegmatite'

Intrusions of pegmatite's ranging in size from a few metres to 50m in diameter are common throughout the study area. There appear to be at least two generations of pegmatite. The first is post D_2 and pre D_3 as S_2 fabrics wrap around the dykes. Both S2 and S3 crosscut the second generation. The mineralogy of both generations of pegmatite is quartz + plagioclase + muscovite ± tourmaline ± biotite.

PLATE 1

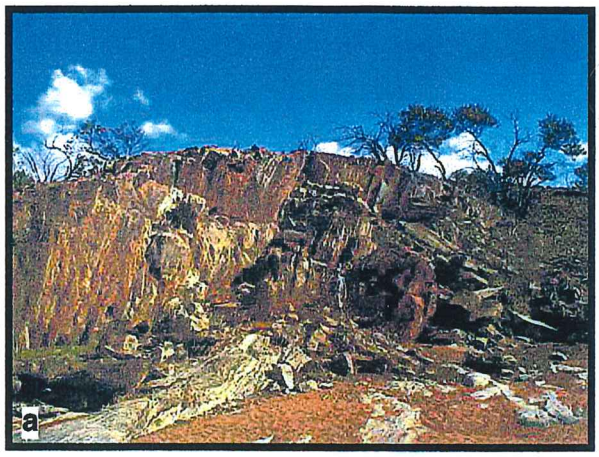

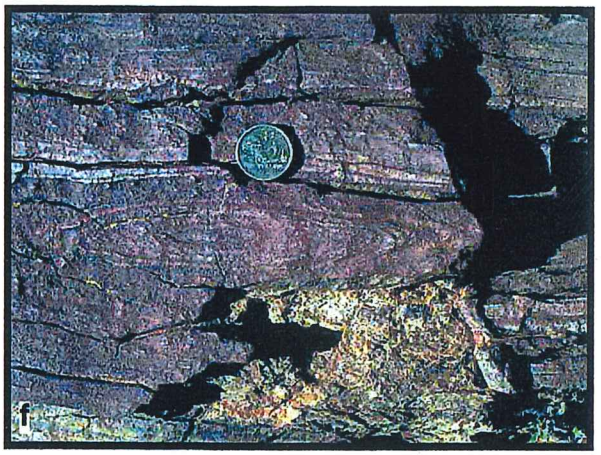

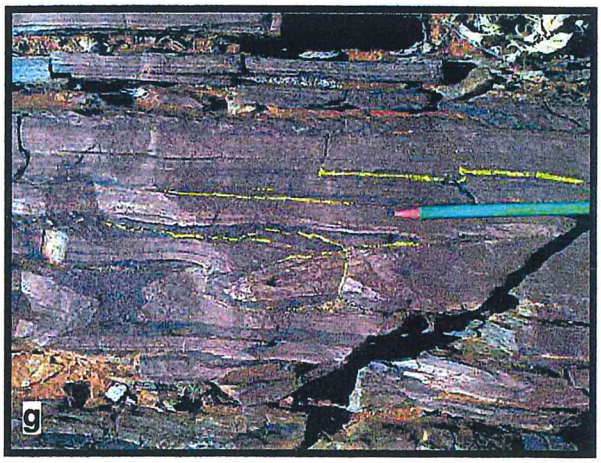

(a) Layering/schistosity
(b) Gneissosity and folding
(c) Boudinage
(d) Boudinage and S-C fabric
(e) F2 parasitic folds and migmatite
(f) Eye-fold in Calc-albite
(g) Shear folding

Chapter 4 Structural Descriptions

This chapter discusses the analysis of structural data including foliations, fold axial planes, shear fabrics and lineations, in order to reconstruct the style and history of deformation in the study area. Figures 4.1, 4.2 and 4.4 show the geometric relation ships of the structural elements defined below.

The high-strain nature of the mapped area, attributed to isoclinal folding and later shearing events, has led to different fold generations reorienting into parallelism, with similar ENE trends. This left recognition of OD$_1$, OD$_2$ and OD$_3$ folds to the spatial relationships of associated fabric elements.

4.1. Origin of Layering

Many of the rocks exhibit a strong gneissosity/layering (Plate 2). In the more albitic units, there are layers that have been so extensively albitised that any S_0 features have been obliterated. This layering appears to be related to the preferential alteration of specific lithologies be hydrothermal fluids. Due to the high degree of transposition in the area this layering is also extensively deformed. Different lithologies deform to different extents based on rheological differences (figure 4.6). One deformation event produces fabrics that appear different in some lithologies with respect to others (plate 2). Field evidence, such as graded and reverse graded bedding, would suggest that the majority of layering represent S_0, which in some lithologies is extensively altered.

4.2. First Deformation (OD$_1$)

4.2.1. Folding

Structural evidence in the form of vergence relationships depicted in figure 4.1, shows that there is a consistent sinistral vergence between S_0 and S_1, which is consistent throughout the whole area. This suggests that F_1 has the form of a major, refolded, reclined syncline. The upper limb of this syncline has been eroded off, and comes closest to outcropping in the major F_2 synform, (Cathedral Rock synform). The best explanation for this is that the F_1 axis has been sheared out and eroded. This is shown in cross section (Figure 6.5).

Figure 4.1

CATHEDRAL ROCK AREA, OLD BOOLCAMATA, OLARY AND SUB AREAS (BEDDING {S0} & SCHISTOSITY {S0})

GN MN

MAGNETIC DECLINATION 8

435

436

6449

6448

DOMAIN D

DOMAIN C

DOMAIN B

DOMAIN A

RAVEN HILL MINE

RAVEN HILL SOUTH MINE

MAP LOCATION

N.T. QLD. W.A. S.A. N.S.W. VIC.

South Australia New South Wales Broken Hill Mapped area Olary 0 20 40 Kilometres

SCALE - 1 : 10 000

100 0 100 200 300 400 500 METRES

LEGEND

- Creek
- Track
- Geological Boundary
- Geological Boundary (Inferred)
- Fault/Shear
- Quarry/Mine
- Overturned Fold
- Synform
- Overturned Fold
- Antiform
- 69 Bedding (S0)
- 69 Schistocity (S1)

STRUCTURAL DATA

DOMAIN A

BEDDING (S0) — N — n=5

SCHISTOCITY (S1) — N — n=3

Equal area projection, lower hemisphere

DOMAIN B

N — n=12

N — n=4

Equal area projection, lower hemisphere

DOMAIN C

N — n=45

N — n=21

Equal area projection, lower hemisphere

DOMAIN D

N — n=25

N — n=17

Equal area projection, lower hemisphere

Figure 4.2

DREW HILL - CATHEDRAL ROCK AREA, OLD BOOLCAMATA, OLARY. (CLEAVAGE {S2 and S3})

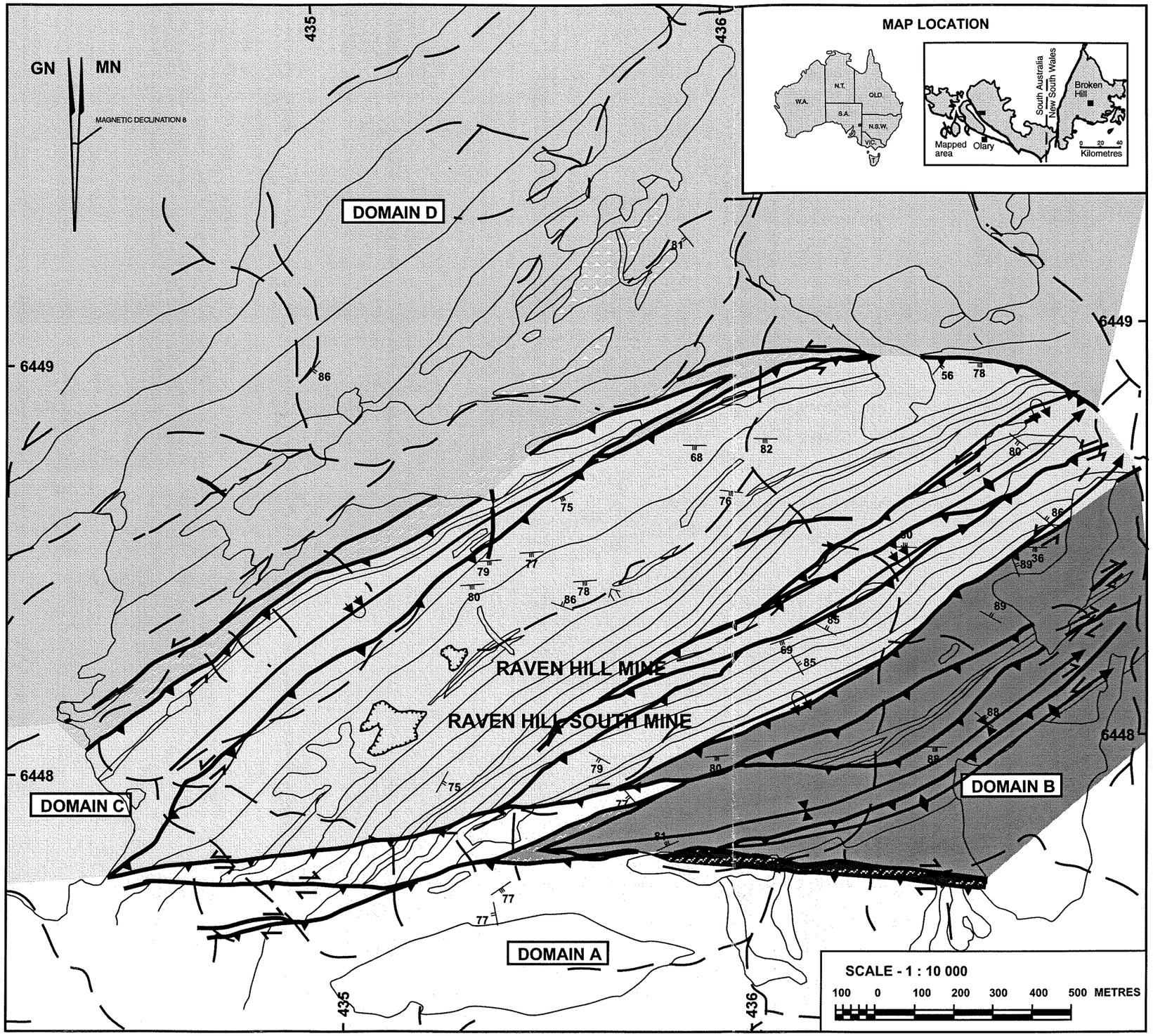

LEGEND

- Creek
- Track
- Geological Boundary
- Geological Boundary (Inferred)
- Fault/Shear
- Quarry/Mine
- Overturned Fold
- Synform
- Overturned Fold
- Antiform
- 69 Cleavage (S2)
- 69 Cleavage (S3)

STRUCTURAL DATA

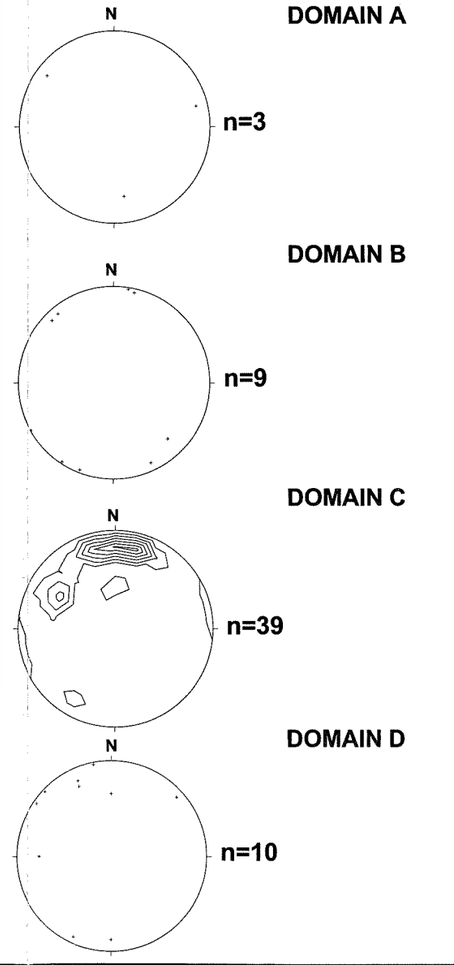

FIGURE 4.3: RELATIONSHIP OF FABRIC ELEMENTS WITHIN CALC-ALBITE

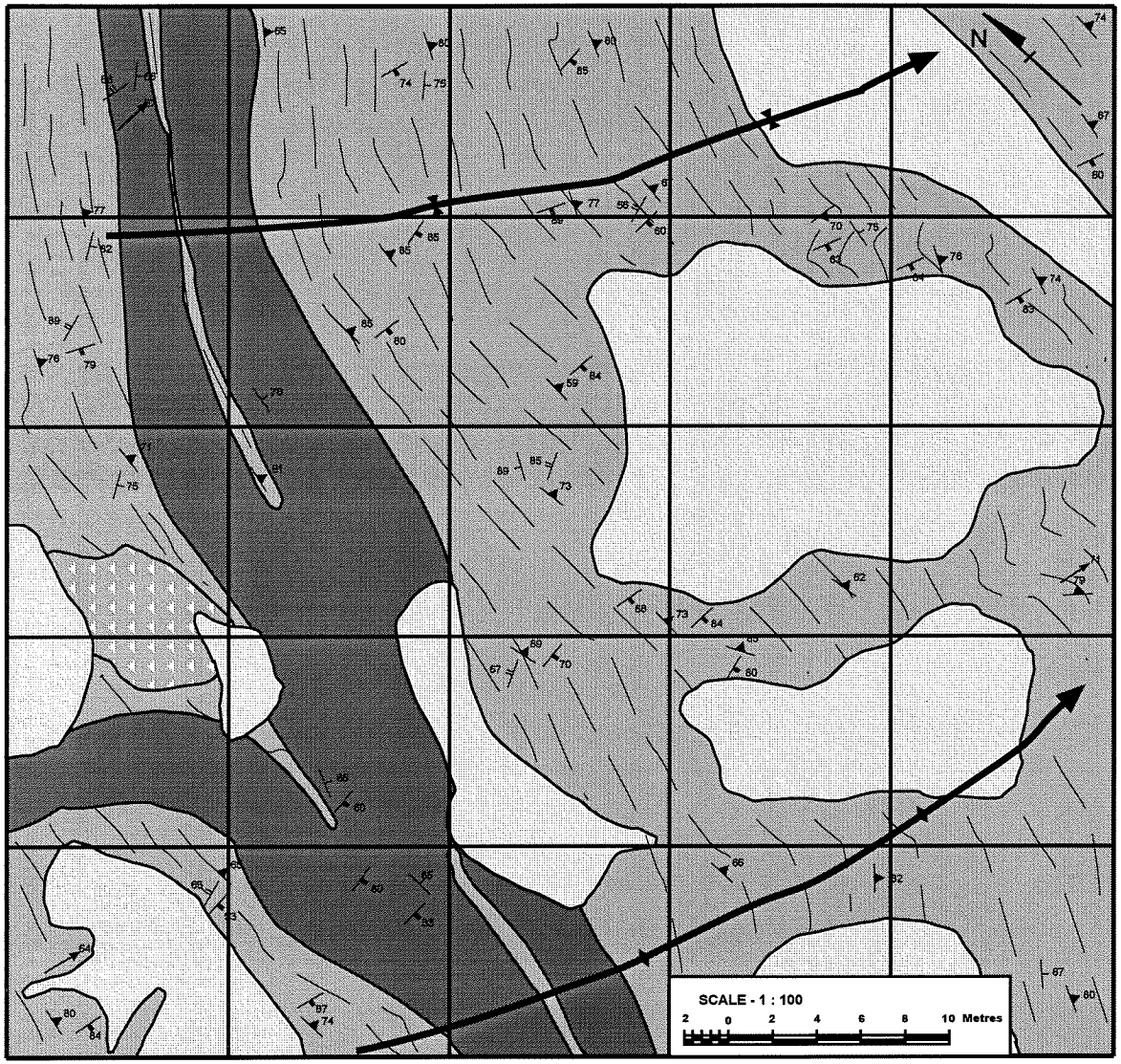

LEGEND

- Boundary
- Bedding (S0)
- Schistosity (S1)
- Cleavage (S2)
- Cleavage (S3)
- Fold
- Intersection Lineation
- Buckling Lineation
- Calc-Albite
- Volcanic
- Alluvium
- Breccia

STEREOGRAM'S

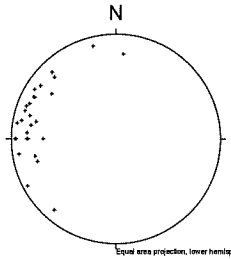

Bedding (s0)

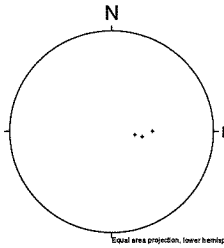

Lineations

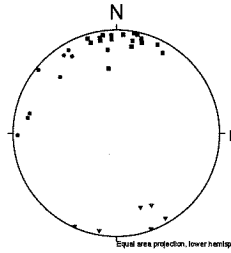

Cleavage
- =S3
- =S2
- =S1

4.2.2. Foliations

S_1 is the earliest recognisable fabric. It is parallel or sub-parallel to S_0, which makes recognition difficult. Many units exhibit an intense gneissosity/layering. Whether or not this layering is S_0 is discussed in section 4.1. In outcrop, S_1 is distinguished by the alignment of magnetite and biotite. In thin section it is distinguished by the alignment of platy minerals such as biotite, muscovite, and sillimanite. In more quartzitic units, S_1 is defined by heavy mineral (magnetite) banding.

S_1 seems to be oriented in a consistently sinistral sense with respect to S_0. This suggests there may be an F_1 fold nappe to the north (antiform) or to the south (synform). This will be discussed further in section 4.3.

4.2.3. Lineations

Several different types of lineations are found throughout the region. Each associated with separate deformation events. Figure 4.4 shows the geometric distributions of linear elements throughout the study area.

L_1 mineral lineations have been obliterated by subsequent deformation. However, where S_0 and S_1 are distinguishable from each other, intersection lineations can be measured (figure 4.4). These are highly variable in their orientations due to the highly transposed nature of the area.

4.3. Second Deformation (*O*D_2)

4.3.1. Folding

OD_2 is the most prominent deformation event in the area. F_2 is represented by isoclinal, ENE trending, overturned folds with a plunge between 60° and 75°. This represents the refolding of the lower limb of the major F_1 syncline mentioned above. S_2 fabrics are highly variable (Figure 4.2). This is due to the effects of the *O*D_3.

Figure 4.4

GEOLOGY OF DREW HILL - CATHEDRAL ROCK AREA, OLD BOOLCAMATA, OLARY. (LINEATION DATA)

GN MN

MAGNETIC DECLINATION 8

435

436

6449

6448

DOMAIN D

DOMAIN C

DOMAIN B

DOMAIN A

RAVEN HILL MINE

RAVEN HILL SOUTH MINE

MAP LOCATION

N.T.
QLD
W.A.
S.A.
N.S.W.
VIC.
South Australia
New South Wales
Broken Hill
Mapped area
Olary
0 20 40
Kilometres

SCALE - 1 : 10 000

100 0 100 200 300 400 500 METRES

LEGEND

- Creek
- Track
- Geological Boundary
- Geological Boundary (Inferred)
- Fault/Shear
- Quarry/Mine
- Antiform
- Overturned Fold
- Synform
- Overturned Fold
- 69 Crenulation Lineation (L3)
- 69 Plunge of Parasitic Fold (Vergence, s, z or m)(L2)
- 69 Mineral Elongation Lineation (L3)
- 69 Intersection Lineation (L1)

STRUCTURAL DATA

DOMAIN A

N

n=7

- SLIP LINEATION (L3)
- INTERSECTION LIN (L1)
- PLUNGE (L2)
- CRENULATION LIN (L3)
- MINERAL STRETCHING (L3)

DOMAIN B

N

n=12

DOMAIN C

N

n=31

DOMAIN D

N

n=30

Figure 4.5 shows parasitic folding in the hinge of a major F_2 fold. These show refolding of F_1 folds. It shows a plunge of 68° towards 120°.

4.3.2. Foliations

A foliation associated with OD$_2$ appears to be the most dominant structure represented in outcrop. The second foliation is most likely associated with OD$_2$. S_2 is axial planer to the major isoclinal, overturned S_2 folds (F_2) which trend ENE throughout the mapped area. These foliations are predominantly found in the hinges of F_2 folds and in F_2 parasitic folds (Plate 1b). S_2 foliations crosscut S_1 foliations, this is particularly evident in crenulated fold hinges of F_2 parasitic folds. These foliations are generally defines by the alignment of muscovite, biotite, chlorite and magnetite. D_2 has also rotated D_1 garnets in some pelitic units (Plate 4).

4.3.3. Lineations

Crenulation lineations (L_2) which have developed in more pelitic units represent the major linear elements formed during OD$_2$. The reorientation of S_1 and the growth of muscovite, perpendicular to the crenulation define these lineations.

4.4. Third Deformation (OD$_3$)

4.4.1. Folding

S_3 fabrics are largely invariable (figure's 4.2 and 4.3). F_3 consists of E-W trending tight to open folds superimposing earlier F_2.

4.4.2. Foliations

A consistently E-W spaced fracture cleavage is found in more competent lithologies. This has been attributed to OD$_3$. In the more pelitic units a crenulation formed at right angles to a lineation defined by muscovite. This lineation trends roughly 40° towards 090°. OD$_3$ deformation is broadly represented by E-W trending open to tight upright folds superimposed on F_2 folds. OD$_3$ is also attributed to the development of retrograde shear zones (Szpunar, 1997) and associated shear folding. These shear zones truncate F_2 fold hinges (Plate 2a). OD$_3$ appears to be the most difficult event to define.

Figure 4.3 shows the relationship of all fabric elements in the Laminated Feldspar rock (calc-albite). Appendix A shows the location for this grid map.

4.4.3. Lineations

L_3 appears to be the most prominent set of lineations throughout the area. OD$_3$ buckling and shearing is responsible for the formation of crenulation lineations and slip (mineral elongation) lineations. These down-dip lineations are usually defined by the alignment of muscovite and minor chlorite and biotite. OD$_3$ thrusting has produced many fabrics typically associated with shear zones. These features are discussed in section 4.6.

4.5. Shearing

Shearing appears to be the most prominent deformational feature in the Cathedral Rock - Drew Hill area. Anastomosing shear zones crosscut the area truncating many structures. Field evidence suggests that shearing post-date's OD$_2$. F_2 structures are truncated by shearing (Plate 2h). Shearing occurs within and between basement lithologies. Field evidence and thin section analysis (chapter 6) suggest that these shear zones represent south over north, steep reverse thrusts, with minor lateral movement. Mineral assemblages within shear zones are typically retrograde, being of lower grades than peak metamorphic assemblages.

The main shear zones within the study area are the Drew Hill and Cathedral Rock shear zones. The implied geometry of these features is represented in figure 6.5.

4.6. Discussion

The structural analysis of the region is generally consistent with the regional framework determined by previous workers. The following section attempts to compare and contrast the findings of this study with those of previous investigations.

Field evidence supports the hypotheses of three Olarian deformations. The most pervasive deformation was associated with OD$_2$ producing moderate to steeply plunging, east-northeast trending isoclinal folds. OF$_2$ appears to have transposed an earlier deformation (OD$_1$). No fold closures associated with OD$_1$ folding are seen within the study area. However, the geometry

FIGURE 4.5: GRID SKETCH IN FOLD HINGE ZONE, CATHEDRAL ROCK CREEK.

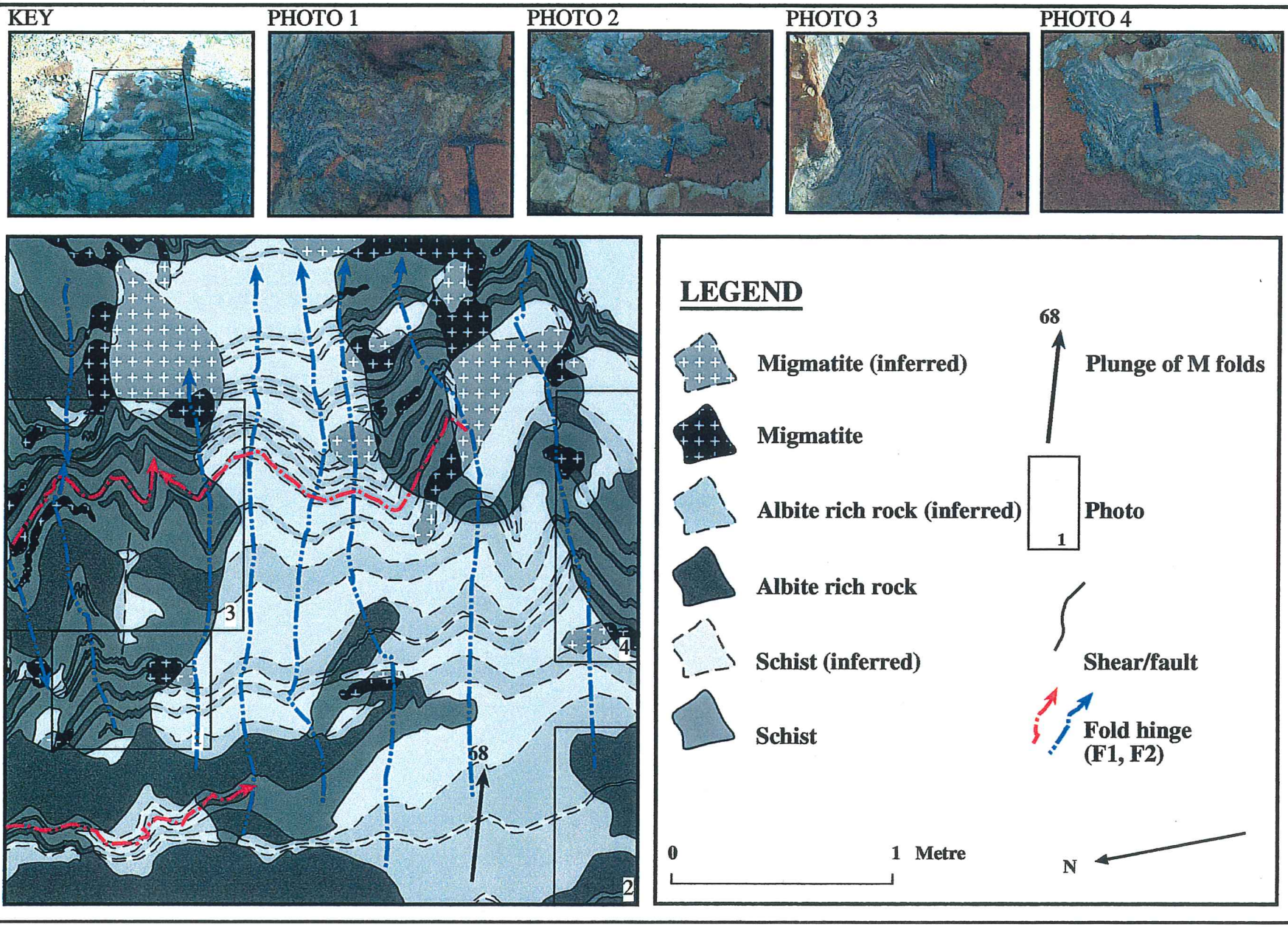

of fabric elements, and work done in an adjacent area, (Taylor, 1999) would suggest that F_1 occurs as a refolded, moderately plunging, reclined isoclinal fold. The F_1 fold closure would occur south of the study area. The northern, or bottom limb of this major fold, would be shallowly dipping, and the southern or upper limb would be more steeply dipping, suggesting a north west sense of vergence. This is contradictory with the finding of Clarke *et al.* (1986), who suggested that the first deformational event resulted in the formation of a regional recumbent fold or nappe complex. The transport direction of this nappe complex was southeast.

The second deformational event appears to have the opposite transport direction as the first. Second generation folds, have steeper northern limbs suggesting a northward sense of vergence. This is also consistent with the formation of basement thrusts associated with OD_3. These thrusts also indicate a northward transport direction (figure 4.5). These thrusts appear as ductile shears ranging from 2-40 metres in width. The area appears to be bounded by two major shears. These are possibly reactivated by Delamerian deformation. An aeromagnetic anomaly seems to indicate that the Cathedral rock shear (see figure 3.1) is continuous with the shear zone which deforms both Willyama and Adelaidean supergroup rocks, that occurs near Mawson Hut, Old Boolcoomata (Ashley *et al*., 1998).

Figure 4.6: Folding and migmatite formation in Quartzofeldspathic gneiss

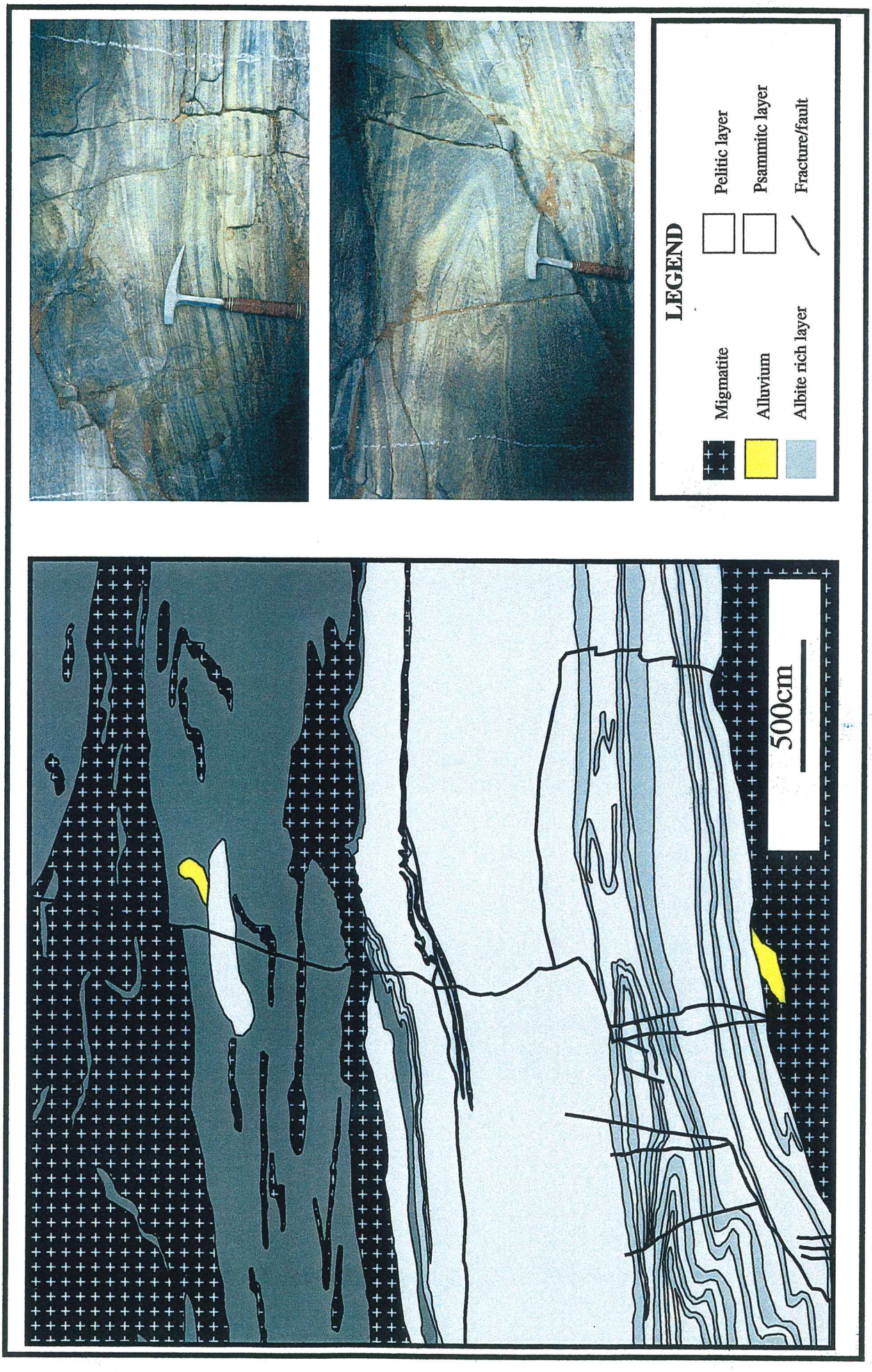

Plate 2

(a) Migmatites and Albite alteration

(b) Migmatites folded and cross-cut by F_2 . Axial trace defined by hammer handle.

(c) Albite Alteration

(d) Shear zone truncating F_2 fold

(e) Shear zone in quartzofeldspathic gneiss

(f) Folding in quartzofeldspathic gneisses

(g) Discrete shear offsetting Albite rich layer

(h) Second generation parasitic folds

PLATE 2

a

b

c

d

e

f

g

h

Chapter 5 Metamorphism and Alteration

The Cathedral Rock - Drew hill area is typical of high-grade gneiss terrains as it has been subject to high metamorphic grade. This area preserves a complex metamorphic history, including metasomatism and local melting. These will be discussed in detail in this chapter.

5.1. Metamorphism

Remnant mineral assemblages from peak metamorphic conditions suggest that upper amphibolite to lower granulite facies metamorphism was achieved during OD_1. During the associated prograde metamorphism, any hydrous phases would have been replaced by anhydrous phases. Field evidence for this consists of partial melt pockets formed within the rocks and these 'migmatites' are discussed further in section 5.3.

Peak metamorphic assemblages appear to have been largely overgrown by later, retrograde assemblages. This is attributed to the influx of hydrous fluids, which are associated with the growth of hydrous minerals in retrograde assemblages.

Clarke et al (1987) subdivided the OD into 4 metamorphic zones, namely 1, 2, 2a and 3 (figure 2.2). Observations by Cook (1993) suggest that some modifications apply to these zones, however Ashley et al. (1998) suggests that the general distribution of these zones appear to be correct. The Cathedral Rock - Drew Hill area falls within zone 2b. Peak metamorphic assemblages observed within metapelites, typically consist of andalusite, K-feldspar, quartz ± garnet and minor muscovite. Clarke et al. (1987) inferred that the P-T-t path for the OD is anticlockwise. The peak metamorphic conditions synchronous with OD_1 reflect a maximum of upper amphibolite grade. This is consistent with thin section analysis, as S_2 fabrics wrap around OD_1 garnets.

Most peak metamorphic assemblages are overprinted by retrograde mineral assemblages, particularly in areas of high strain. Hydrous phases such as muscovite are consistent with syn-post OD_2 retrogression. There appears to be two major retrograde metamorphic events. These mineral assemblages are observed in shear zone fabrics, where there appears to be two generations of muscovite (plate 5). These shear zones are associated with syn and post (Delamerian) OD_3 deformation. S_3 fabrics that include muscovite, truncate S_2 fabrics, also containing muscovite. The first generation of muscovite is possibly related to exhumation

during OD_2. The second generation of muscovite is possibly related to the influx of hydrous fluids associated with OD_3 and post-OD_3 shearing. This will be discussed further in section 5.2.

Harley (1989) proposed a scheme of common metamorphic reactions in pelitic rocks found in high-grade gneiss terrains (figure 5.1)

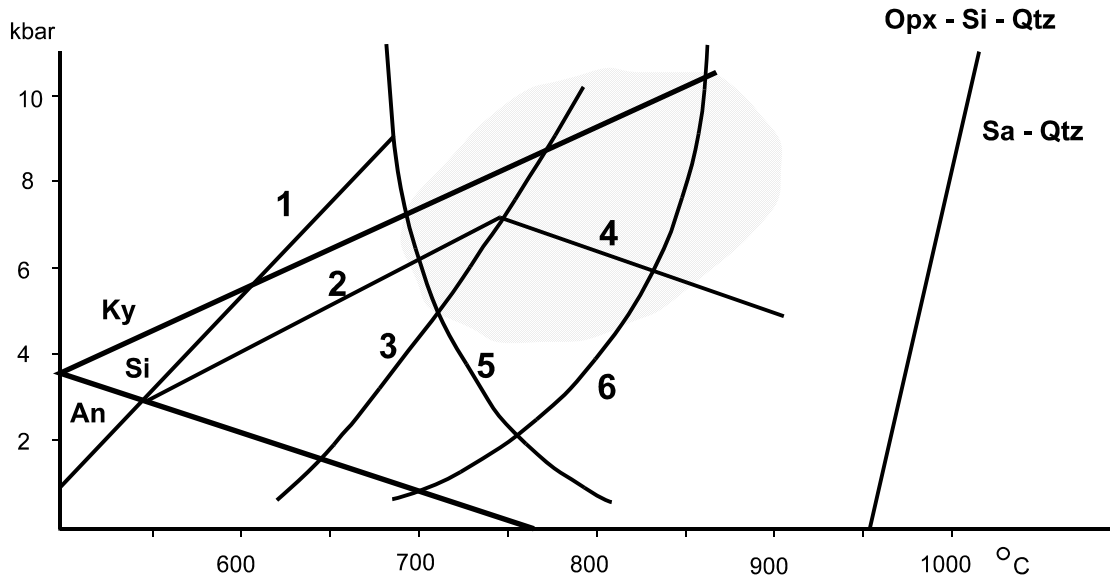

Figure 5.1: Petrogenetic P-T grid showing common reactions in pelitic rocks at high-grade metamorphic conditions. The grey field represents the range of most commonly encountered conditions in high-grade gneiss terrains Harley (1989) and Passchier *et al.,* (1990).

The reactions associated with the curves in figure 5.1 are*;

1. Mu + Q = Kf + Als + V
2. Bi + Als + Q = Cd + Kf + V
3. Bi + Als + Q = Ga + Cd + Kf + V
4. Cd = Als + Ga + Q + V
5. Ph + Q = Kf + En + melt
6. Plag + Q + Kf + V = melt
7. Plag + Q + Kf = melt

*The Abbreviations used are: Als –Al-silicate; An –andalusite; Bi –biotite; Cd –cordierite; En –enstatite; Ga –garnet; Ilm –Ilmenite; Kf –K-feldspar; Ky –kyanite; Mu –muscovite; Opx –orthopyroxene; Plag –plagioclase; Q –quartz; Sa –saphrine; Si –sillimanite; V –vapour

Reaction one or six would be consistent with post retrogression mineral assemblages. The presence of co-existing quartz, K-Feldspar and Al-silicates would be consistent with reaction 1 (Passchier *et al.,* 1990). Muscovite appears afterwards as a secondary mineral associated with retrogression. The second scenario which is consistent with reaction six would be explained by the presence of partial melts (migmatites). The formation of migmatites is discussed in section 5.2.

5.2. Migmatite Formation

Migmatite formation is common amongst the psammopelitic units within the study unit. There appear to be two main generations of migmatites within the rocks. Figure 4.5 and 4.6 show the field relationships of these migmatites with their host rocks. The first generation of migmatites are pre OD_2, as F_2 parasitic folds (figure 4.6) fold them. These possibly formed as a result of prograde upper amphibolite facies metamorphism synchronous with OD_1 (section 5.1). These were likely to have formed in situ, as some exhibit leucocratic melt segregations of immiscible components. The second generation of migmatites are syn-post OD_2 as they cross cut S_2 fabrics (figure 4.5). Whilst the majority of these second-generation migmatites appear to be injected, some exhibit textures associated with in situ partial melting. The second generation migmatites possibly formed synchronously with OD_2 and continued afterwards for some time, as some appeared to be deformed in part by OD_2 as well as cross cutting the fabrics (Plate 2b).

The formation of migmatites appears to be restricted to psammopelitic layers (figure 4.7), whereas the more albitic layers exhibit little to no partial melting. The derivation of hydrous fluids from the breakdown of hydrous minerals would be associated with this migmatite formation. Fitzsimons (1995) suggests that these fluids are derived either by solid-state dehydration reactions or by dehydration melting reactions, at higher metamorphic grades. The second scenario is likely to be the case within the study area. The reason for this is that retrograde assemblages appear to form sometime after the melting. With solid-state dehydration the fluids are released immediately, whereas hydrous melt components are stored within the dissolved component of the melt phase (Fitzsimons, 1995). These fluids would have been released in a delayed burst during retrogression pre-syn OD_2, as the fluid reached water saturation. Retrogression is mainly concentrated in high strain zones such as shear zones. This is consistent with the release of hydrous fluids, which would have used the zones as conduits for transport and crystallisation.

5.3. Alteration

Many of the rocks within the study area have been subject to varying extents of hydrothermal alteration. This alteration is evident in the form of extensive albitisation and growth of minerals such as magnetite and minor actinolite. Albitisation is attributed to a regional scale alteration event which is characterised be Na(Fe) alteration (Ashley et al., 1998).

Many of the rocks particularly those associated with high strain are largely recrystallised, with K-feldspar being replaced with albite. This is attributed to Na-K cation exchange in the feldspar (Szpunar, 1997). Orthoclase ($KAlSi_30_8$) is replaced by albite ($NaAlSi_3O_8$) in the following chemical reaction: $KAlSi_3O_8 + Na^+ = NaAlSi_3O_8 + K^+$. By adding Sodium to the system the reaction shifts to the right. Szpunar (1997) suggests this could be attributed to sodium chloride associated with seawater.

Fe alteration is exhibited in the growth of magnetite, particularly in shear zones and more highly strained units. The presence of magnetite, an Fe^{3+} bearing mineral, is indicative of oxidising conditions.

The Cathedral Rock Calcsilicate matrix breccia shows some extent of Ca alteration. Evidence for this is by the growth of Ca bearing minerals such as actinolite. Sampling of the Cathedral Rock breccias was prohibited so the mineralogy could not be described.

Chapter 6 Strain Analysis

This chapter describes the methods used to measure strain variation within the study area. These include fold profiles, Rf/ϕ analysis, δ-angle analysis, microstructural analysis and cross-section balancing. Each of these methods provides a limited quantification of strain, but will be combined to provide an overall picture of strain variation within the study area.

6.1. Fold profiles

Mesoscopic scale folds are abundant throughout the study area. The majority of the folds are Class 2 folds (Ramsay, 1967), exhibiting parallel dip isogons, thickened hinges and thin limbs. Class 1c folds are also formed within some lithologies. The majority of these folds appear to be flattened. The degree of apparent strain can be measured using the Hudleston method of analysis (see Appendix B), for determining the amount of flattening of class 1c folds. The folds used in this analysis are shown in plate 3. These consist of three class 1c folds, which have suffered some degree of flattening. Fold 1 comes from comes from the *'migmatised quartzofeldspathic gneisses and schists'* unit. Fold 2 comes from the *'laminated fine grained calc-albitite'* unit. Fold 3 lies in the same stratigraphic position as fold 2, approximately 400m ENE. The relative locations of these samples are shown in appendix B. The $\sqrt{\lambda_2}/\sqrt{\lambda_1}$ values determined for folds 1, 2 and 3 are 0.2, 0.3 and 0.3 respectively. The percentage of shortening for each of these folds was calculated (Appendix B). Fold 1 gave a value of 82.1% for apparent total minimum shortening. This is significantly greater than the values obtained for folds 2 and 3, which were 51.7% and 51.2% respectively. The similarity in the shortening values for folds 1 and 2 may be explained by their near identical stratigraphic position, considering the principle stress direction is near perpendicular to the main layering. The shortening value obtained for fold 1 was significantly larger. The *'migmatised quartzofeldspathic gneisses and schists'* unit appears to have deformed to a larger extent than other lithologies.

PLATE 3

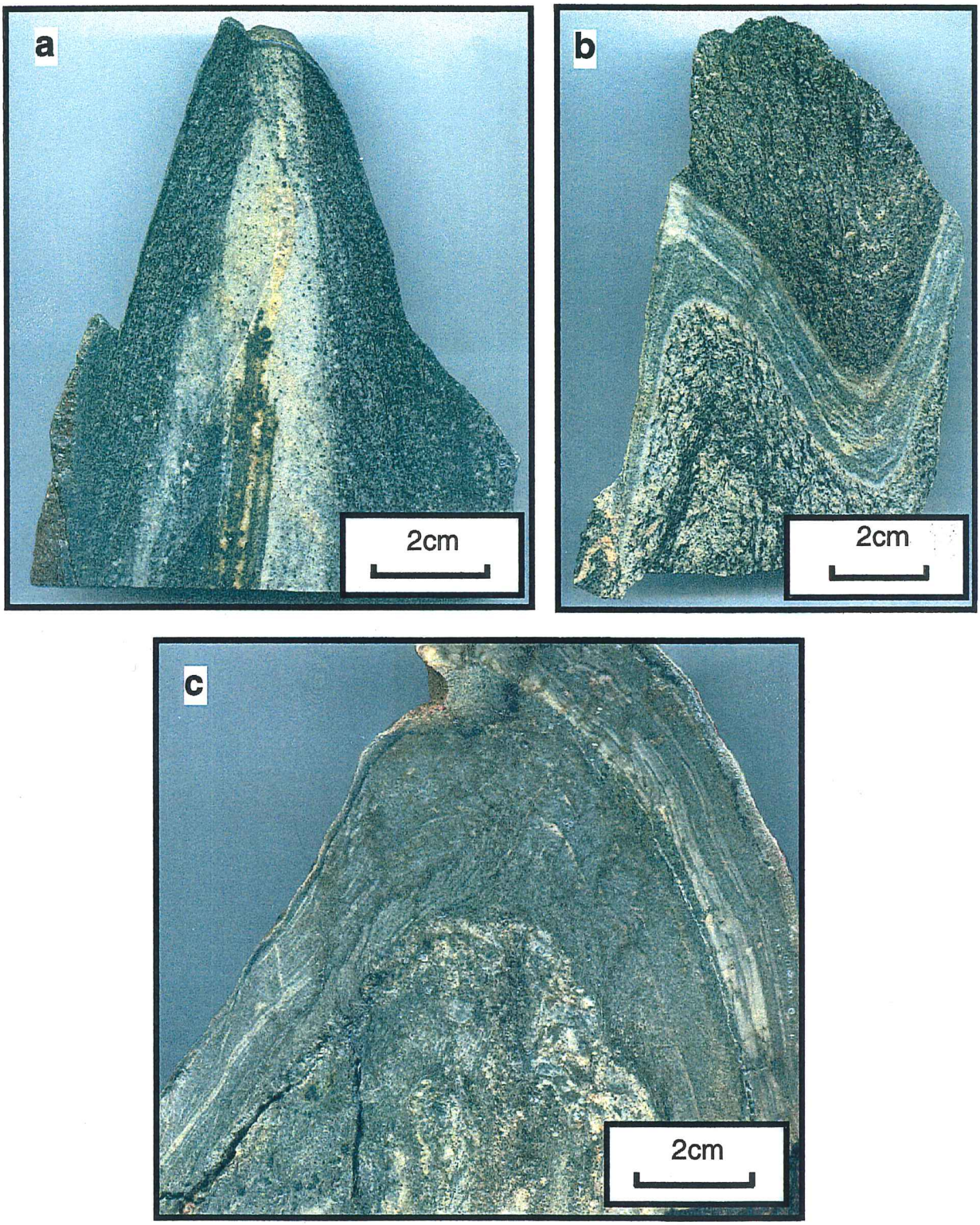

(a) Fold 1 from *migmatised quartzofeldspathic gneiss*

(b) Fold 2 from *laminated fine grained calc-albitite*

(c) Fold 3 from *laminated fine grained calc-albitite*

6.2. Rf/ϕ Analysis

The Rf/ϕ (see Appendix B) was applied to deformed quartz and feldspar crystals in samples taken from the study area. Each oriented sample was cut along the XZ and YZ planes. Thin sections were taken from each plane and photomicrographs taken of relevant crystal aggregates. The deformed grains were then measured using 'DIGITISE' (McEachran, 1989). Rf/ϕ scatter plots were produced using 'INSTRAIN' (Erslev, 1989). 'INSTRAIN' is a computer program, designed to analyse the x and y coordinates of the points stored in ASCII (text only) format, such as those input via 'DIGITIZE'.

In each sample the x-axis was defined by the elongation lineation which lie within the main foliation (XY) plane. The results for the Rf/ϕ analysis are shown in table 6.1. The dimensions of the strain ellipsoid were calculated (Appendix B) and plotted on a Flinn diagram (Fig. 6.1). All samples show a strong degree of flattening or oblate strain, plotting in the field of apparent flattening as represented by their associated k-values (see table 6.1). Many of the samples were recrystallised which, depending on the timing, would have affected the dimensions of the real strain ellipsoid. This would give a smaller value for the degree of shortening. This will be discussed further in section 6.6.

6.3. δ-angle Analysis

The δ-angle refers to the angle formed between layering and schistosity. This method is based on the assumption that this angle will be affected be strain. There are many other factors, which would determine the angle formed between layering and schistosity. The most obvious of these is the proximity of a reading to a fold hinge. Due to the isoclinal nature of folding within the study area, the majority of readings are taken from the limbs of these folds. Ramsey and Huber (1987) describe the method for determining the angle between two planes (Fig. 6.2). The significance of the δ-angle is not represented well in literature, and further study is required to deem it useful.

TABLE 6.1: SUMMARY OF RESULTS FOR Rf/Φ DATA

Sample	XZ				YZ				Ri			Rs			k-value
	Rfmin	Rfmax	Ri	Rs	Rfmin	Rfmax	Ri	Rs	X	Y	Z	X	Y	Z	
A1121-3	1.204	3.423	1.686127	2.030097	1.102	2.41	1.478828	1.629669	1.686127	1.478828	1	2.030097	1.629669	1	0.390223
A1121-6	1.218	3.964	1.804028	2.197306	1.217	2.576	1.454882	1.770591	1.804028	1.454882	1	2.197306	1.770591	1	0.312749
A1121-10	1.312	5.47	2.041864	2.678925	1.162	2.382	1.431752	1.663696	2.041864	1.431752	1	2.678925	1.663696	1	0.919435
A1121-12	1.305	2.683	1.433854	1.87118	1.22	2.303	1.373938	1.676204	1.433854	1.373938	1	1.87118	1.676204	1	0.172019
A1121-16	1.351	3.439	1.595469	2.155479	1.234	2.752	1.493367	1.842815	1.595469	1.493367	1	2.155479	1.842815	1	0.201309
A1121-2	1.235	3.642	1.717262	2.120818	1.228	3.04	1.573394	1.932128	1.717262	1.573394	1	2.120818	1.932128	1	0.10477
A1121-G	1.116	2.528	1.505069	1.679657	1.192	2.125	1.335185	1.59154	1.505069	1.335185	1	1.679657	1.59154	1	0.093596

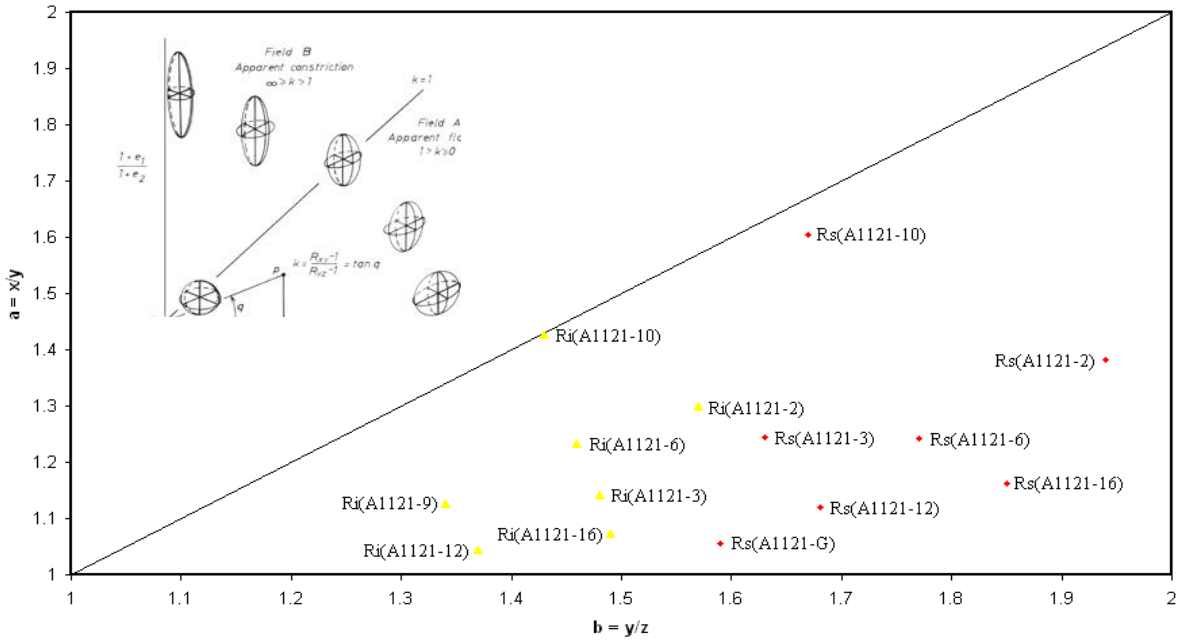

Figure 6.1: Flinn diagram displaying the strain fields associated with different samples. Inset after Ramsey and Huber (1987)

The delta angle measurements for the structural data were determined using *Stereonett®*, a free-ware program designed for the analysis of structural data. This data is tabulated in appendix B. These angles were plotted in their relative positions on the map of the study area and contoured at 0-5, 5-10, 10-15, 15-20, 20-25 and 25-30+ angle increments (Fig. 6.3). The average δ-angle for the area is 17.5° The majority of data (~80%) yielded angles below 20°. This is consistent with the high strain nature of the area. In terms of fold style, it is also consistent with isoclinal folding. There are two main regions of high δ-angle readings. One of these lies in close proximity to an F_2 fold hinge. The other lies around the Cathedral-Rock breccias. The three main regions of low δ-angle readings (<10°) coincide with areas of high strain. One of these anomalies coincides with the highly strained *'psammopelite and muscovite schist'* unit. The other two coincide with major shear zones (Cathedral rock shear zone and Drew hill shear zone).

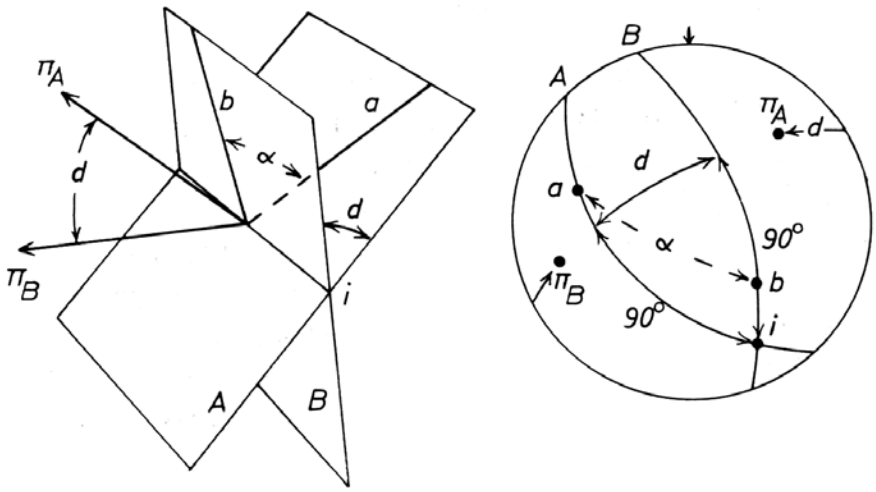

Figure 6.2: The Geometric features arising from the intersection of two planes A and B and their representation on a projection. Ramsey and Huber (1987).

On its own, the δ-angle is relatively useless and its real use is as a qualitative representation of strain. It is best coupled with other methods. A comparison of all strain analysis performed on the study area will be presented in section 6.6.

6.4. Microstructural Analysis

Thin sections were taken from oriented samples and analysed for their petrological, mineralogical and microstructural relationships. The locations of these samples are shown in appendix B. Most of the samples used for microstructural analysis were taken from shear zones or areas of intense strain. These were analysed for kinematic indicators (see plates 4 and 5). These kinematic indicators were used to confirm the sense of movement on major structures such as the Cathedral-Rock and Drew-Hill shear zones.

Highly strained rocks of the *'platy schist'* unit contain mica fish and rotated garnets (plate 4a-e). S_2 and S_3 muscovite crystals wrap around these garnet porphyroblasts. This indicated that the garnets are pre-OD$_2$ possibly coincident with syn-OD$_1$ peak metamorphic conditions. Chlorite crystals also occur in the pressure shadows of these rotated garnet crystals, also indicating pre-OD$_2$ peak metamorphic conditions. These porphyroblasts and their recrystallised tails are useful in the determination of the sense of shear in zones of high strain (see Simpson and Schmid, 1983; Lister and Snoke, 1984; Passchier and Simpson, 1986). All kinematic indicators give a south over north sense of movement. The relict garnet

FIGURE 6.3: DELTA ANGLE DATA SUPERIMPOSED ON THE GEOLOGYOF THE DREW HILL - CATHEDRAL ROCK AREA

porphyroblasts exhibit both δ- and σ-type kinematic indicators of Passchier and Simpson (1986), (Fig. 6.4). Plate 4b and 4c show examples of these types of porphyroblasts. The presence of certain proportions of these clasts depends on the rate of recrystallisation *R* to shear strain rate γ. With large amounts of recrystallisation, the flow of recrystallised material within the tails is constantly supplemented. As a result σ- type, wedge shaped tails are formed. With a lesser degree of recrystallisation, the tails are supplied with an insufficient quantity of recrystallised grains to thicken the wedge, so a narrow tail is formed of the δ- type is formed, with the tail being dragged around the rotated host grain. The majority of the garnets within the thin sections exhibited σ- type tails. This shows that recrystallisation is prominent.

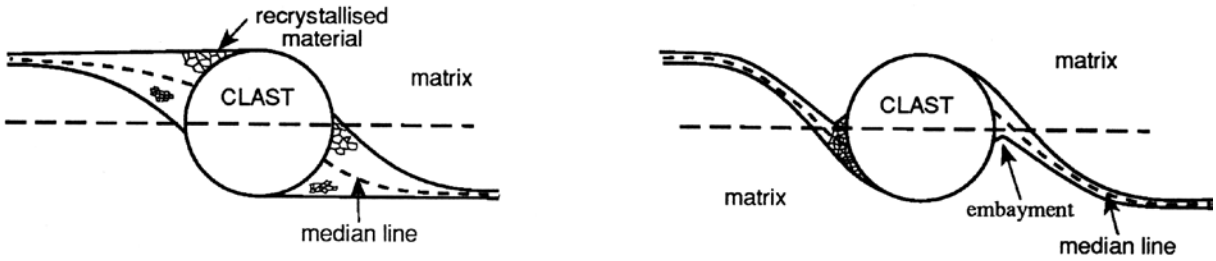

Figure 6.4: δ- and σ-type indicators (after Passchier and Simpson, 1986)

Outside shear zones the rocks still exhibit features indicative of high strain. These include quartz ribbons and quartz crystals, which exhibit undulose extinction and the formation of sub-grains (plate 4f). Many of these micro-fabrics are similar to those described by Martelat *et al.* (1999) for deformed granulite- to high-amphibolite facies quartzofeldspathic rocks in southern Madagascar. Plate 4f shows an example of a quartz crystal exhibiting undulose extinction and the formation of sub-grains. In finer grained lithologies the grain boundaries of sub-equant feldspar and quartz grains are straight and meet in triple point junctions. These matrices are cross cut be thin quartz ribbons, typically 1-2mm wide. This is characteristic of the type-1 fabric of Martelat (1999)

The most prominent microstructures are found within the shear zones that crosscut the study area. These consist of both phyllonitic fabrics (eg. Drew hill shear zone) and more schistose and mylonitic fabrics (eg. Cathedral Rock shear zone). Thin section of oriented samples taken from the Drew hill shear zone (plate 5a to c) exhibit classic S-C fabrics. These fabrics also give a sense of movement, which in this case is south over north, indicating a thrust style of deformation.

Due to their fine-grained nature and high degree of recrystallisation, it is difficult to define any sense of movement within ultra-mylonites. Thin (<3m) bands of ultra-mylonites are common within the more albitic units, particularly the *'laminated feldspar'* unit. Under higher magnification and plane polarised light (plate 5d) extensional crenulation cleavages are evident. Platt and Vissers (1980) describe these features. Extensional fractures form as shear bands along the older foliation.

6.5. Cross Section Balancing

A two dimensional cross-section was constructed perpendicular to the general layering of the study area (Fig 6.5). Due to the lateral movement of the Cathedral Rock shear zone during the Delamerian orogeny, the balancing and restoration of this cross section may be invalidated (McCross, 1988). Due to the lack of three dimensional control on structures with a strike-slip component, any real values for shortening are referred to the section X-Y, which lies between the Cathedral Rock and Drew Hill shear zones (see figure 6.5). Keeping these limitations in mind, if we assume that volume is conserved, an estimate of the depth to the decollement can be determined. Under constant volume conditions, the amount of material uplifted will equal the decrease due to shortening. De Sitter (1964) and Dahlstrom (1969) proposed a method for calculating the depth of the crustal decollement (Fig 6.6). Using this method the depth of the crustal decollement was determined to be approximately 1km below the surface. The degree of shortening of the packet of sediments represented between points X and Y (Fig. 6.4) was determined to be approximately 65%. The resultant restored section was achieved by unfolding the layers between the Cathedral Rock and Drew Hill shear zones and removing the portrayed displacements associated with each. The difference in thickness of the layers on either side of the Cathedral Rock shear zone is attributed to Delamerian displacement. For this reason layers to the north of this structure were not used in calculating the percentage of shortening.

The restored section represents the post $O D_1$ and pre $O D_2$ stratigraphic relationship. The position of the F_1 axial trace is shown on the unrestored section in figure 6.5, and is described in more detail in chapter 4.

FIGURE 6.5: VIABLE CROSS SECTION AND BALANCED RECONSTRUCTION: CATHEDRAL ROCK - DREW HILL AREA

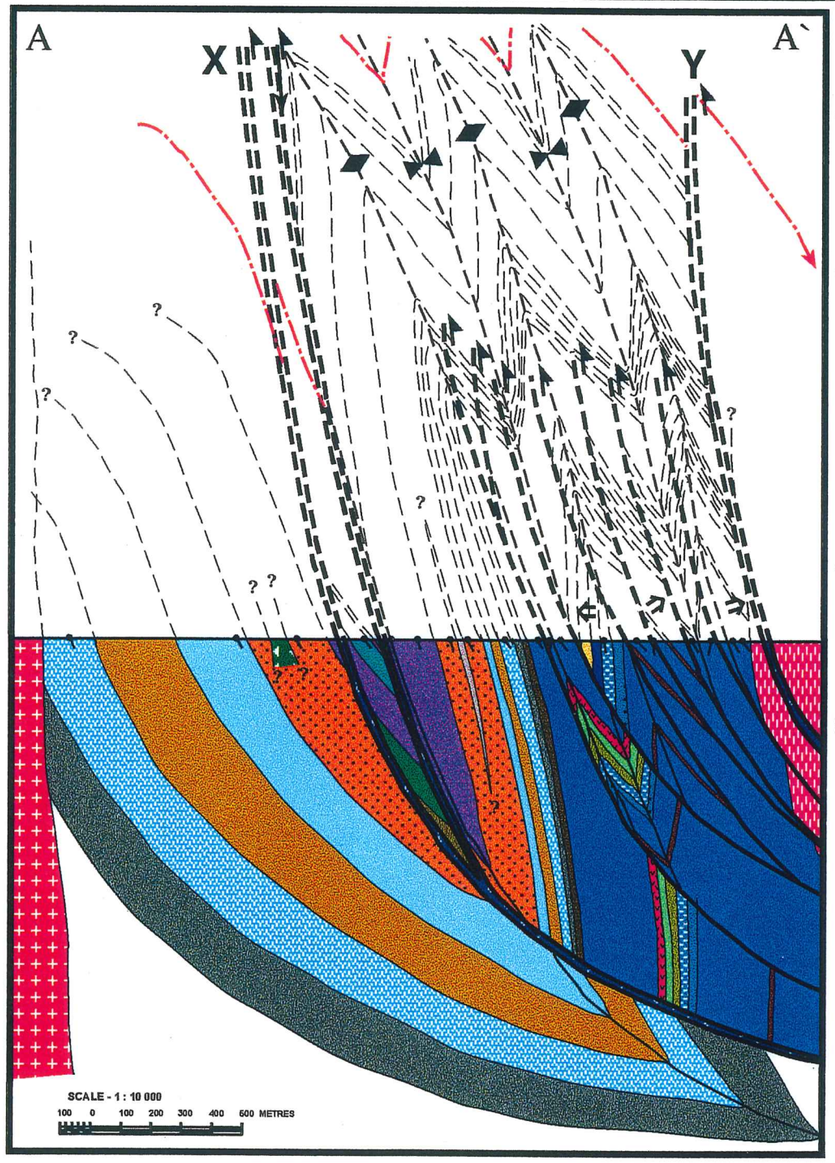

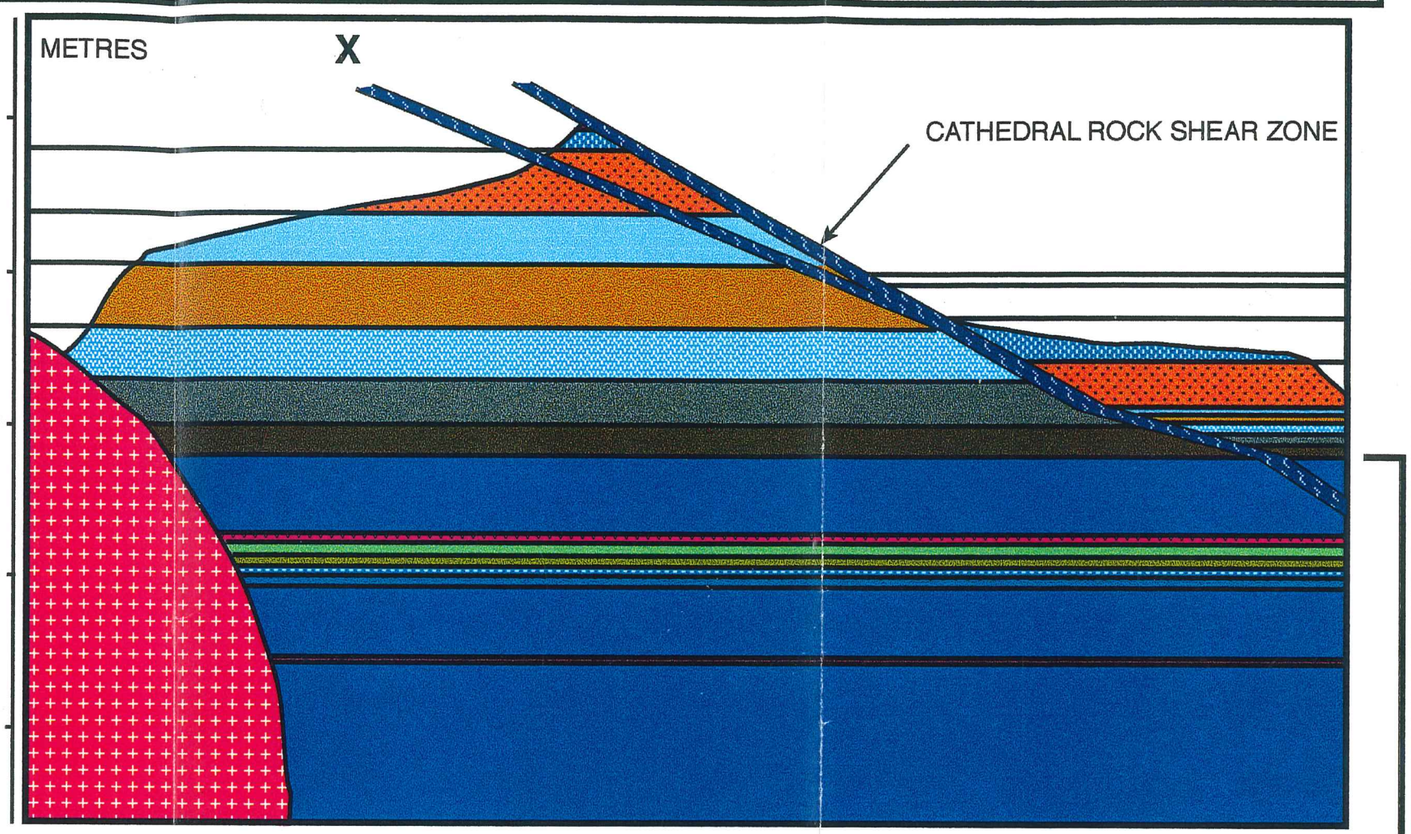

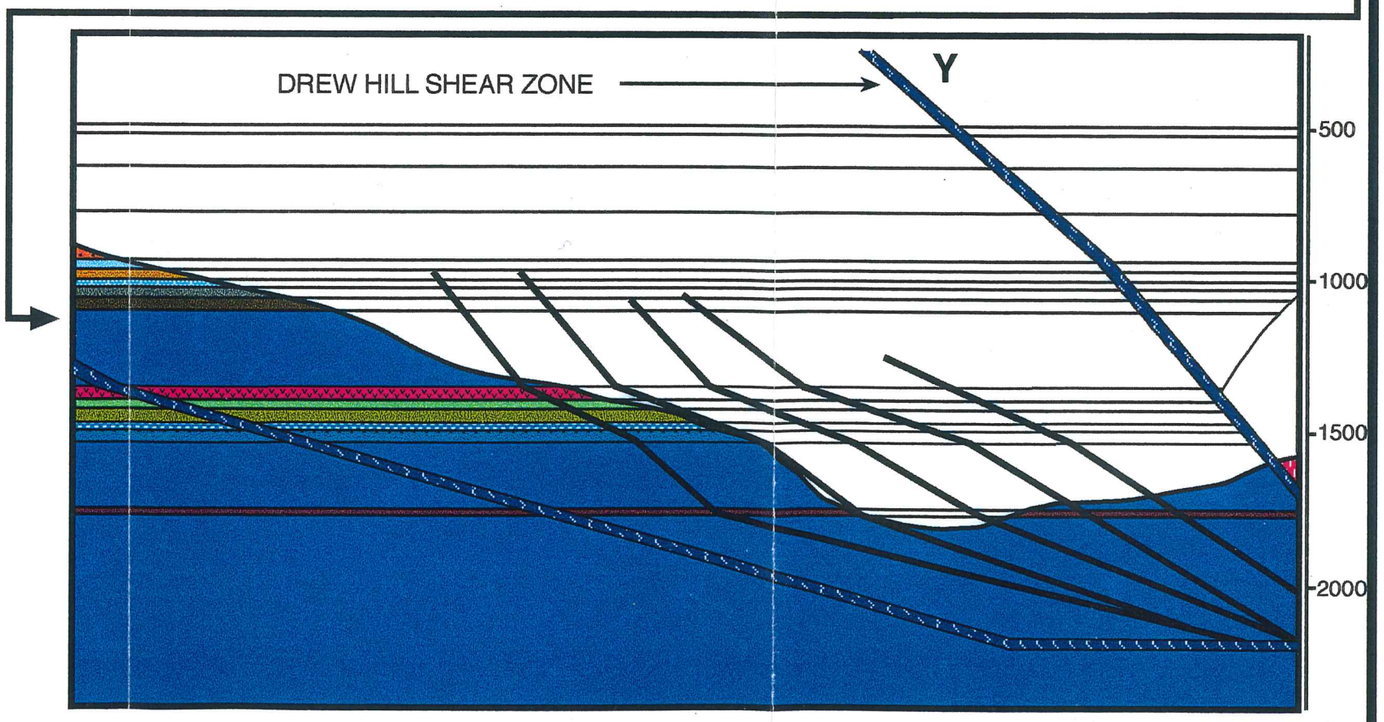

LEGEND

- ANTIFORM } F2
- SYNFORM } F2
- DIP OF BEDDING
- BOUNDARY
- DISCRETE SHEAR
- SHEAR ZONE
- YOUNGING
- F1 AXIAL TRACE

REFER TO FIGURE 3.1 FOR LITHOLOGY'S AND POSITION OF CROSS SECTION

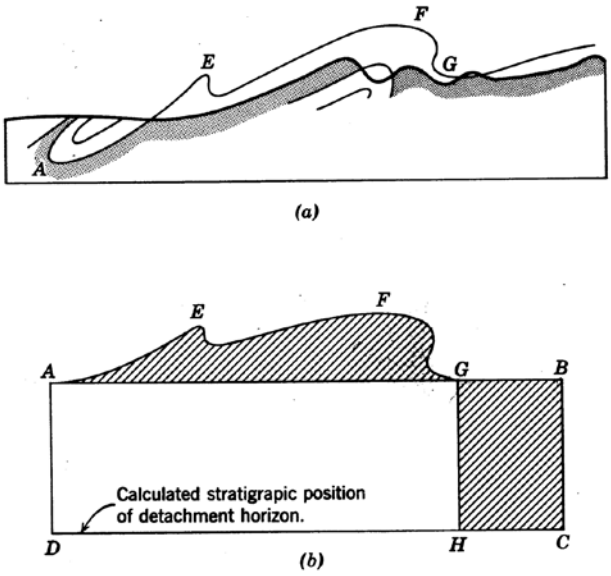

Figure 6.6: Calculation of depth of folding. (After Ragan, 1973)

6.6. Discussion

The strain analysis on the study area has shown that the region of greatest strain occurs between the Cathedral Rock and Drew Hill shear zones. Cross section restoration showed that this area has undergone approximately 65% shortening. Within this area strain fluctuated according to numerous factors. A variation in shortening due to folding appears to be related to lithological variation. Class 1c folds from older quartzofeldspathic rocks appear to have undergone more flattening than folds in younger albitic units.

Rf/phi analysis showed there to be little variation in strain state across the study area. All samples gave a value for total minimum shortening between 27.6 and 39.4% shortening. The relative consistency of this data may be explained by recrystallisation. Most of the samples have been extensively recrystallised. This would give a much smaller value for shortening as the original strain ellipse would be overprinted by another possibly less deformed one.

Kinematic indicators were used to determine the sense of movement of major structures within the area. It should be noted that the cross section has been restored to post OD_2. This would suggest that overall this package of rocks has undergone a much larger degree of shortening.

Figure 6.7 is a representation of all data from the strain analysis with respect to major structures. There are four major delta angle lows. Three of these occur between the Cathedral

Rock and Drew Hill shear zones. Two of these are correlated with the structures themselves, the other correlates with the laminated feldspar unit on the southern side of the Cathedral Rock shear. This zone is extensively mylonitised. Just north of the Cathedral Rock synform is a major positive delta angle anomaly. This correlates with the position of the Cathedral Rock Breccias. These breccias are possibly associated with extension perpendicular to the principal stress direction.

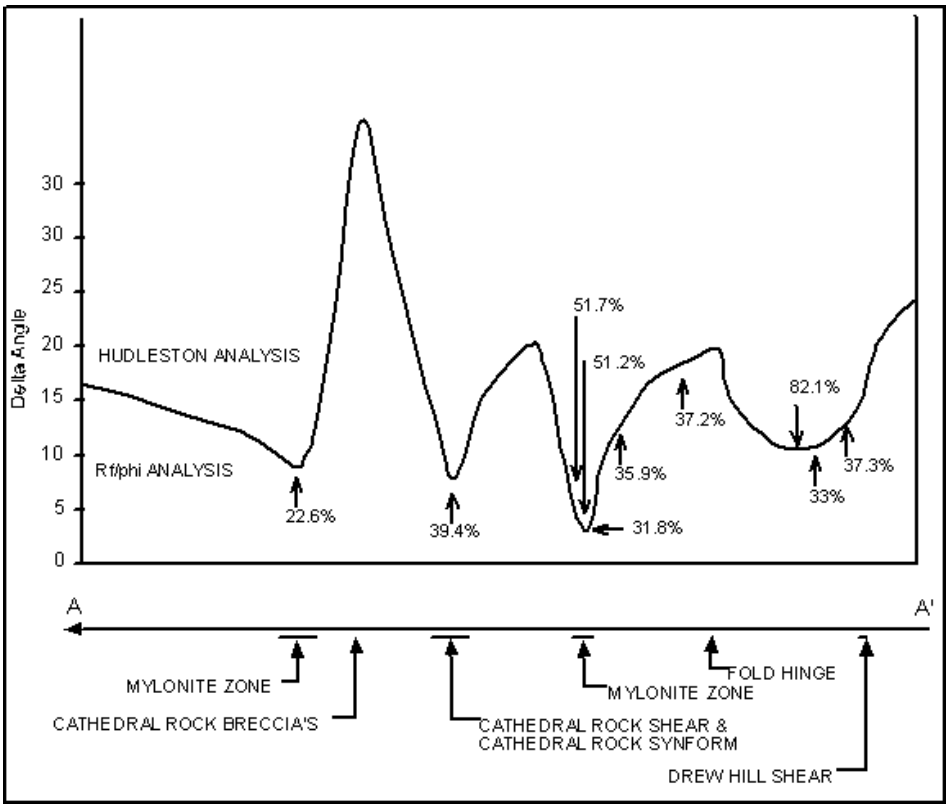

Figure 6.7: Representation of strain across major structures along transect A-A'.

PLATE 4

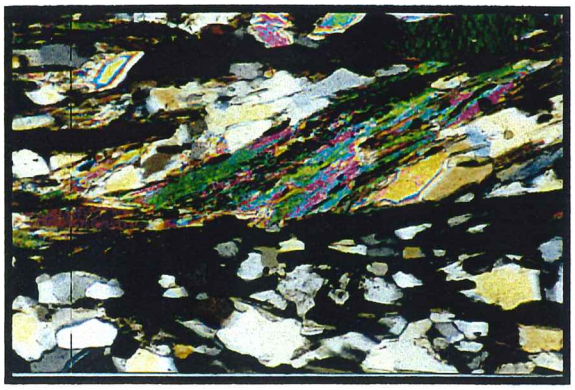

a

b

c

d

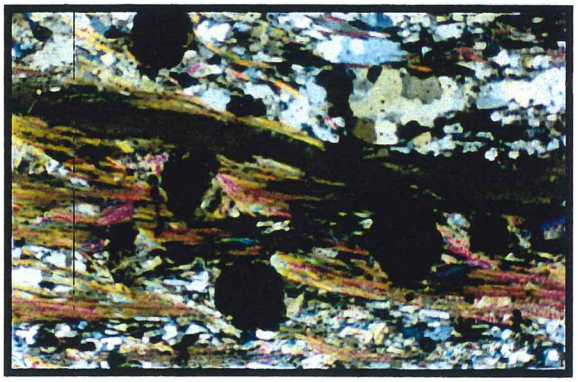

e

f

(a) Mica fish in '*platey schist*' unit

(b) Rotated δ- type garnet in *'platy schist'* unit

(c) Rotated σ- type garnet in '*platy schist*' unit

(d) Garnet porphyroblast with recrystallised chlorite tail

(e) Group of rotated garnets in '*platy schist*' unit

(f) Quartz exhibiting undulose extinction and the formation of sub grains

All photos at same scale **1mm**

PLATE 5

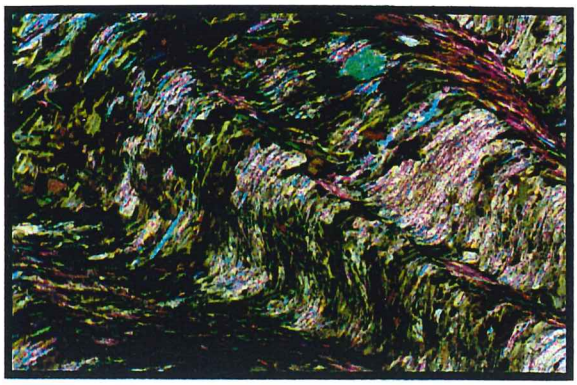

a

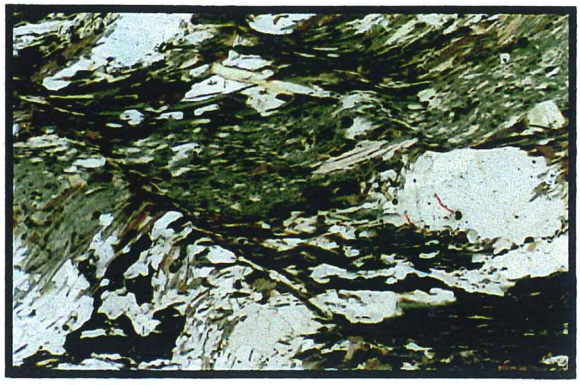

b

c

d

e

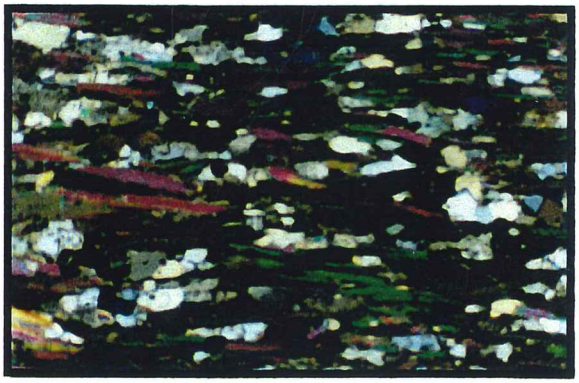

f

(a) S-C fabric developed in Drew Hill shear zone

(b) S-C fabric wrapping around quartz grain

(c) Further S-C fabrics

(d) Extensional crenulation cleavage in ultra-mylonite

(e) YZ section of crunulations formed in '*platey schist*' unit

(f) Same rock type as in (e) except in XZ plane

All photos at same scale 1mm

Chapter 7 Tectonic Model and Interpretations

Structural analysis of the area (chapter 4) and cross section restoration (chapter 6) would suggest that F_1 originally consisted of tight to isoclinal NW verging folds. Subsequent deformation (OD$_2$ and OD$_3$) has refolded F_1 and thrusting of older strata on top of younger strata is attributed to the last phase of Olarian deformation.

7.1. Tectonic Model for the Cathedral Rock – Drew Hill Area

The OD is interpreted to be part of a failed Paleo-proterozoic rift system (Willis *et al*., 1983). Rifting of Archaean basement produced the basin in which the Willyama supergroup sediments were deposited. Associated with rifting were the intrusion of granitiods (Fig. 7.1a). Granitiods outcropping within the study area have been interpreted to pre date Olarian deformation (Constable, 1999).

Menpes (1992) proposed a tectonic model for the structural evolution of a transpression zone in the southern Adelaide fold belts. Although Delamerian in age, this model is very similar to the model proposed for the Willyama complex (Fig.7.1)

The geometry of folding produced by OD$_1$, can be interpreted by initial thin-skinned thrusting (Fig. 7.1b). For this model to work there must by a horizon within the lower sequences of the Willyama super group sediments which is relatively incompetent and acts as a basal decollement. The thrust sheets were carried ‘piggyback’ onto a foreland Archaean shelf towards the northwest. As a result of early thrust stacking, crustal thickening would result in heating of the basement and this is consistent with peak metamorphic assemblages associated with OD$_1$ (chapter 5). Crustal thickening and heating would also weaken the basement and it would become susceptible to ensuing compression. This is consistent with the fact that the reactivation of originally extensional faults into reverse sense thrusts would produce the interpreted geometry of overturned F_1 folds (Fig. 7.1c)

Further shortening would produce a superimposed buckling of these layers parallel to sub-parallel with F_1. This is attributed to OD$_2$ which would have refolded F_1 structures into a geometries such as those represented by the Cathedral Rock F_2 synform (Fig. 7.1d). Further compression led to the further reactivation and propagation of basement thrusts into the

Figure 7.1: Proposed Tectonic Model for the Olary Domain

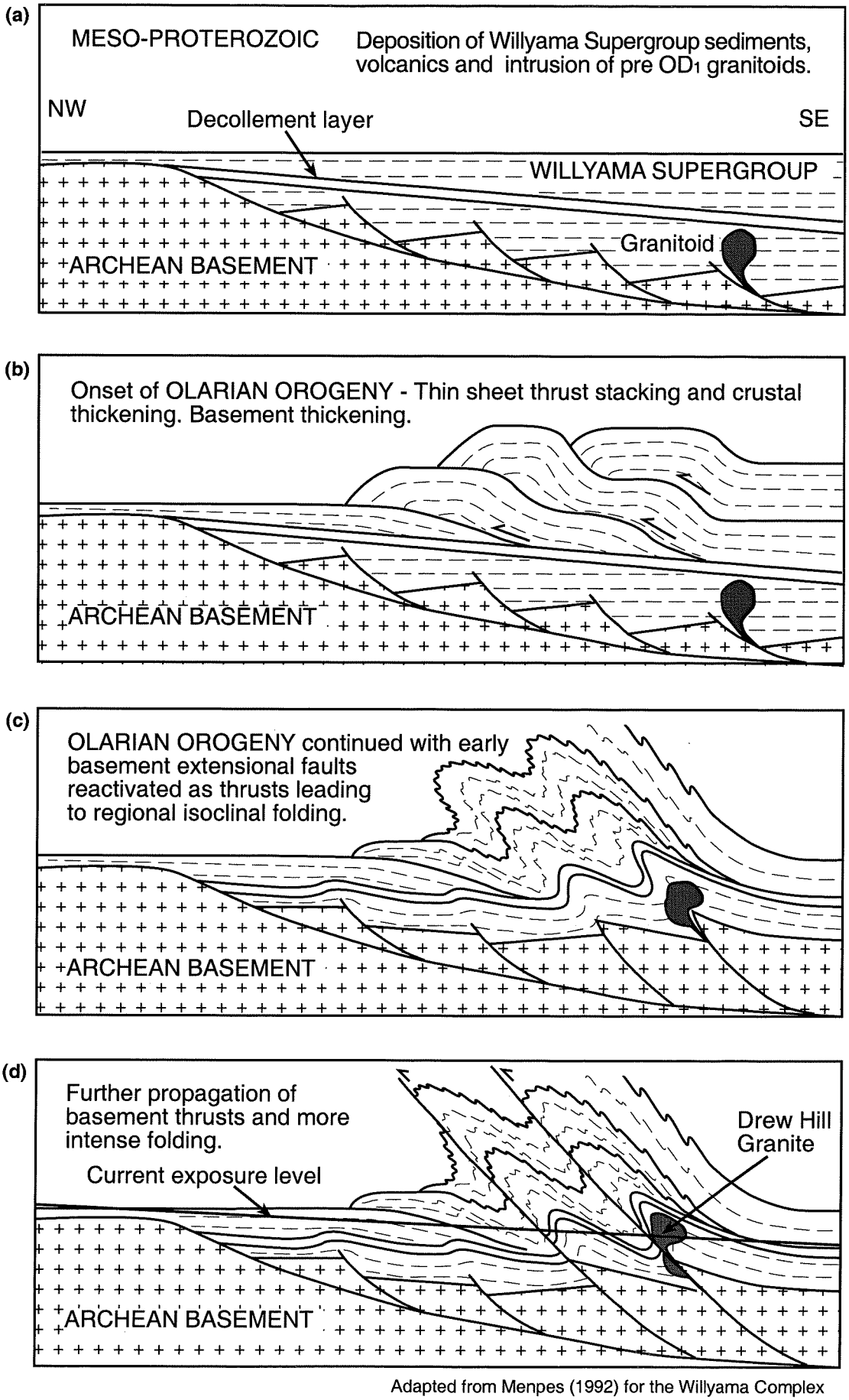

Adapted from Menpes (1992) for the Willyama Complex

deformed metasediments. Further flattening would have occurred and this is associated with the conversion of Class 1b to class 1c folds. This basement thrusting would also be responsible for the exhumation of pre OD_1 granitiods, such as the Drew hill granite, from depth.

This model is based on a few basic assumptions, which lead to a number of complications. One of these is that the geometry of different Olarian deformations differs laterally. In some places there is a minor oblique component to thrusts. The different deformation paths associated with Olarian deformations may be explained by the external boundary displacements of the system, and the internal rheological variation. The later is important in the study area, as strain analysis indicated different lithologies reacted differently to varying deformation styles. This wide variation in rheological properties may have resulted in the complex deformation paths observed in the study area. The consistent oblate nature of the strain ellipsoid reflects that the area is significantly flattened, related to the reactivation of basement faults and further compression.

Figure 7.2 shows a 3-dimensional representation of the structures resulting from the processes described above. The Cathedral Rock – Drew Hill area is interpreted as forming between two major thrusts. This may explain the high strain nature and relative sub-parallelism of structures associated with different deformations.

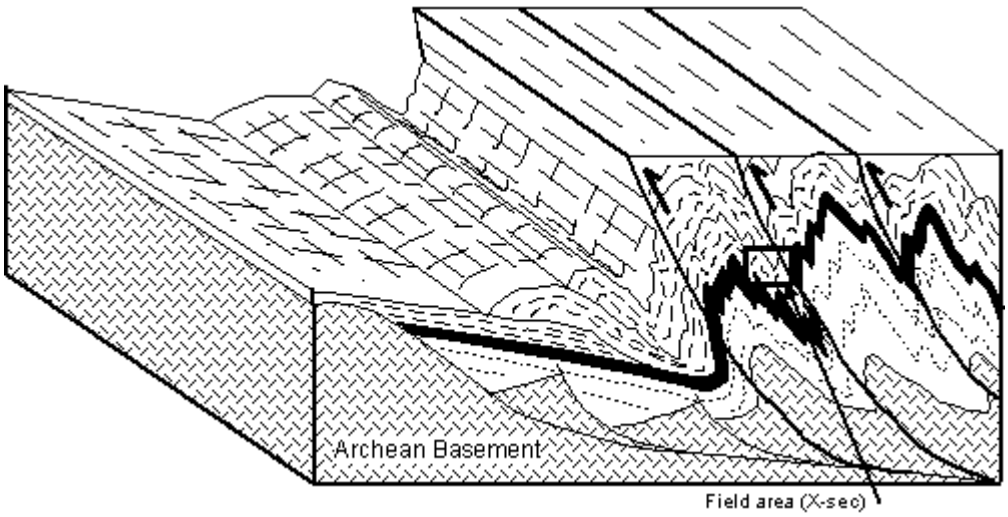

Figure 7.2: Schematic 3-dimensional representation of structures produced in the Olary domain and the relative position of the study area.

Chapter 8 Conclusions

The Willyama Supergroup metasediments of the Cathedral Rock – Drew hill area has been deformed by three major deformational events. Compression resulting in a northwest transport direction firstly produced a thin-skinned duplex terrain. This led to crustal thickening and heating. As a result middle to lower crustal rocks reached high metamorphic grades and deformed plastically in the early Olarian Orogeny. Metamorphic grades and partial melting provided evidence for the timing of major, tectonothermal events. The evidence presented here supports the idea of an initial peak metamorphic grade of upper amphibolite facies followed by two retrograde events associated with the exhumation of supra-crustal rocks and the release of hydrous fluids associated with shearing, respectively.

The reactivation of basement normal faults in a reverse sense as a result of further compression, led to more intense folding and thrusting associated with the later part of the Olarian Orogeny. Field evidence supports previous models of three deformation events through this sequence.

The study area represents a highly strained zone where three deformations have been superimposed into a single structure, the Cathedral Rock synform. This structure represents a second-generation fold that refolds the F_1 axial surface. Consistent vergence relationships across this structure provide important evidence for the transport direction of regional compression.

The most highly strained rocks occur between two interpreted basement thrusts with approximately 60% shortening following original thin sheet thrust stacking associated with OD_1. Strain analysis supported this figure, however due to high levels of recrystallisation, fabrics associated with early deformation are largely overprinted.

REFERENCES

Archibald, NJ, (1980). Old Boolcoomata-Mt Mulga Mine Area, Geology. In: Reports on E.L. 263, 416, 450, 457,767, 848, 1175. Esso Exploration and Production Aust. S. Aust. Dep. Mines and Energy. Open file env. 3360 (unpublished)

Ashley, PM, Cook, N.D.J. and Fanning, C.M. (1996). Geochemistry and age of metamorphosed felsic igneous rocks with A-type affinities in the Willyama Supergroup, Olary Block, South Australia, and implications for mineral exploration. *Lithos*, **38**: pp 167-184.

Ashley, PM, Conor, CHH, Skirrow, RG, (1998). Geology of the Olary Domain, Curnamona Province, South Australia. Field guidebook to Broken Hill Exploration Initiative excursion. Department of Primary Industries and Resources of South Australia. 53pp.

Berry, RF, Flint, RB, and Grady, AE. (1978). Deformation histoty of the Outalpa area and its application to the Olary Province, South Australia. *Transactions of the Royal Society of Australia*, **102**: pp45-53.

Bierlein, FP. (1995). Sulphide mineralisation in the Olary Block, South Australia: A study in element mobility and depositional conditions. Ph. D. thesis, University of Melbourne.

Clarke, GL, Burg, JP, Wilson, CJL, (1986). Stratigraphic and structural constraints on the Proterozoic tectonic history of the Olary Block, South Australia. *Precambrian Research*, **34**: pp107-137

Clarke, GL, Guiraud, M, Powell, R, Burg, JP, (1987). Metamorphism in the Olary Block, South Australia: compression with cooling in the Proterozoic fold belt. *Journal of Metamorphic Geology*, **5**: 291-306

Cobbold, PR, and Quinquis, H. (1980). Development of sheath folds in shear regimes. *Journal of Structural Geology,* **2:** pp119-126.

Constable, SA, (1999). Geological mapping and the geochemical and petrological characterisation of the 'Woman - in – White' amphibolite and associated felsic rocks. *B.Sc Honours thesis*. University of Adelaide.

Cook, NDJ, (1993). Geology of metamorphosed Proterozoic playa lake deposits, Olary Block, South Australia. Ph. D. thesis, University of New England.

Cook, NDJ, and Ashley, PM, (1992). Meta-evaporite sequence, exhalative chemical sediments and associated rocks in the Proterozoic Willyama Supergroup, South Australia: implications for metallogenesis. *Precambrian Research*, **56**: 211-226

Dahlstrom, CDA, (1969). The upper detachment in concentric folding. *Bulletin of Canadian Petroleum Geology*. **17**: pp326-346

De Sitter, LU, (1964). *Structural Geology: second edition*. New York, McGraw-Hill, 551p

Dunnet, D. (1969). A technique of finite strain analysis using elliptical particles. *Tectonophysics*, **7**: pp.117-136.

Erslev, E. (1989). *INSTRAIN – An integrated analysis program for Macintosh.* Rockware Inc.

Fitzsimmons, ICW, (1995). Fluid escape from migmatites – the importance of retrograde deformation. *Halls Gap SGTSG Conference Abstract Volume*. **V** pp62-64

Flint, RB, Parker, AJ, (1993).Willyama Inliers, in Drexel, JF, Preiss, WV, Parker, AJ (eds.) The Geology of South Australia. Volume 1. The Precambrian. *Geological Survey of South Australia*. Bulletin **54**: 82-93.

Hanmer, S, Passchier, C, (1991). Shear-sense indicators: a review. *Geological Survey of Canada*. **90**(17): 72pp

Harley, SL, (1989). The origins of granulites: a metamorphic perspective. *Geol Mag*, **126**: pp215-247

Hobbs, BE. Means, WD, and Williams, P.F., (1979). *An outline of structural geology*. Toronto, John Wiley and Sons, pp571.

Hudleston, PJ. (1973). Fold morphology and some geometrical implications of theories of fold development. *Tectonophysics*, **16**: pp1-46

James, PR, and Clark, IF, (1993). Grid sketching to aid teaching geological mapping in an area of complex polydeformation. *Journal of Geological Education*, **41**: 443pp

Lister, GS, and Snoke, AW, (1984). S-C mylonites. *Journal of Structural Geology*, **6**: pp617-638

Martelat, J, Schulmann, K, Lardeaux, J, Nocollet, C, Cardon, H, (1999). Granulite microfabrics and deformation mechanisms in southern Madagascar. *Journal of Structural Geology,* **21**: pp671-687.

McClay, KR, (1987). The Mapping of Geological Structures. John Wiley and Sons Ltd. England. 161pp

McCross, AM, (1988). Restoration of Transpression/transtension by generating the three-dimensional segmented helical loci deformed lines across structure contour maps. *Journal of Structural Geology*, **10**(1): pp109-120.

McEachran, D. (1989*). DIGITIZE™ - Digitising software for the Macintosh, Version 1*. Rockware Inc.

Menpes (1992). Structural evolution of a transpression zone in the southern Adelaide fold belt: Northeast Dudley peninsula, Kangaroo Island. *B.Sc Honours Thesis.* University of Adelaide.

Passchier, CW, Myers, JS, Kroner, A, (1990). *Field geology of high-grade gneiss terrains*. Springer-Verlag Berlin Heidelberg. 150p

Passchier, CW and Simpson, C. (1986). Porphyroclast systems as kinematic indicators. *Journal of Structural Geology*, **8**: pp831-843.

Passchier, CW and Trouw, RAJ, (1998). *Microtectonics*. Springer. Berlin. 289p

Platt, JP, and Vissers, RLM, (1980). Extensional structures in anisotropic rocks. *Journal of structural geology*, **2**: pp397-410

Ragan, DM, (1973). *Structural geology: an introduction to geometrical techniques, second edition.* John Wiley and Sons , Inc. Canada. P208

Ramsay, JG. (1967). *Folding and fracturing of Rocks.* McGraw-Hill, New . Folding and fracturing of Rocks. McGraw-Hill, New York, pp567.

Ramsay, JG, Graham, RH, (1970): Strain variation in shear belts. *Canadian Journal of Earth Sciences.* **7**: pp786-813.

Ramsay, JG. and Huber, MJ. (1983). *The Technique of Modern Structural Geology. Volume 1: Strain Analysis*. Academic Press London.

Ramsay, JG. and Huber, MJ. (1987). *The Technique of Modern Structural Geology. Volume 2: Folds and fractures*. Academic Press London.

Simpson, C and Schmid, SM, (1983). An evaluation of criteria to deduce the sense of movement in sheared rocks. *Bulletin of the Geological Society of America*, **94**: pp1281-1288.

Stevens, BPJ, Barnes, RG, Forbes, BG, (1990). Willyama Block – regional geology and minor mineralisation, *in* Hughes, FE. (ed.) Geology of the mineral deposits of Australia and Papua New Guinea. *Australiasian Institute of Mining and Metallurgy, Monograph*, **14**: pp1065-1072.

Szpunar, MA, (1997). Structural and Geochemical investigation of Proterozoic crustal evolution in the Weekaroo area, Olary Domain, South Australia. *B.Sc Honours Thesis*. University of Adelaide.

Taylor, AD, (1999). The structure mapping adjacent to the 'Woman in White' Amphibolite, Olary Domain, South Australia. *B.Sc Honours Thesis*. University of Adelaide.

Tourignay, G, Tremlay, A, (1997). Origin and incremental evolution of brittle/ductile shear zones in granite rocks: natural examples from the southern Abitibi Belt, Canada. *Journal of Structural Geology*. **19**(1): pp15-27

Willis, IL, Brown, RE, Stroud, WJ, Stevens, BPJ, (1983). The early Proterozoic Willyama Supergroup: stratigraphic subdivision and interpretation of high to low-grade metamorphic rocks in the Broken Hill Block, New South Wales. *Journal of the Geological Society of South Australia*, **30**: pp195-224

Wiltshire, RG, (1975). The structural geology of the Old Boolcoomata area. *Ph.D Thesis*, University of Adelaide.

APPENDIX A: Sample and photo localities

Locality map

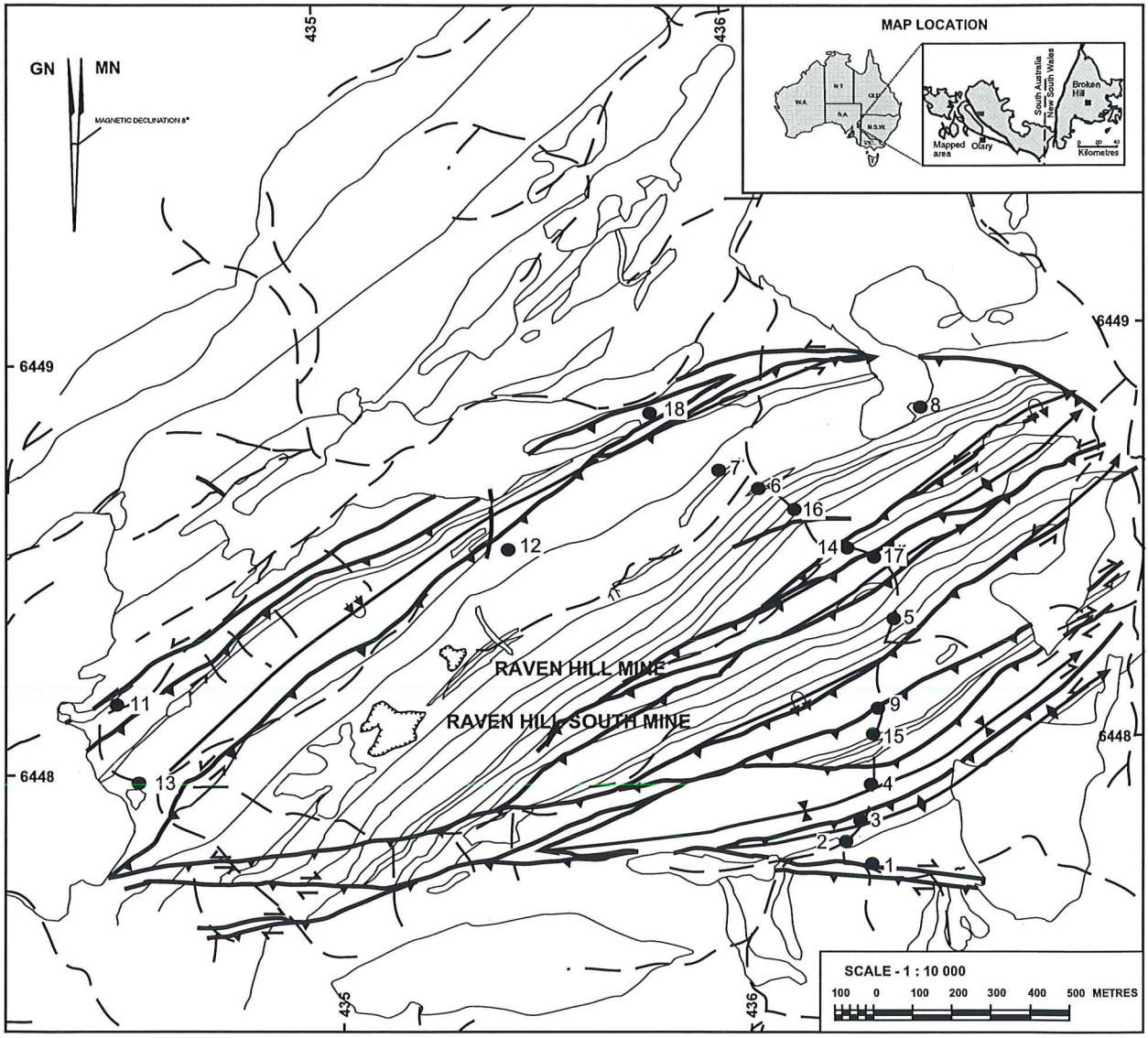

Table of localities

Location	sample number	plate number	figure number
1	A1121-2	1c and 5a-c	
2			4.5
3	A1121-3		
4	A1121-11	3a and 4f	4.6
5	A1121-16		
6	A1121-6		
7	A1121-B	3b	
8	A1121-12 & 13	1f-g, 2f and 3c	
9		1b-e, 2g	
10	A1121-Q	4a-e	
11	A1121-G	5d	
12	A1121-21	5e-f	
13	A1121-10		
14		1a	
15		1c	
16		2b-c	
17		2d	
18			4.3

APPENDIX B: STRAIN ANALYSIS TECHNIQUES

HUDLESTON ANALYSIS

The Hudleston method for analysing the flattening of mesoscopic scale folding uses fold isogon angles to determine an apparent X/Z ratio. This method relates the parameters ϕ and α which are defined in figure B1.a. The relationship (α-ϕ versus α) is plotted onto a mathematically derived set of curves. This relationship defines a line with a slope representative of a specific X/Z ratio (figure B1.b). Hudleston (1973) suggests that this method yields only an 'apparent' strain and is based upon one major assumption. This is that the fold styles were initially class 1(b) styles of Ramsey (1967), which have been subjected to a bulk flattening strain under homogeneous, pure shear conditions to develop class 1(c) styles. The major use of this method is to determine the relative variation in magnitude of the finite strain associated with flattened folds. The value obtained ($\sqrt{\lambda_2}/\sqrt{\lambda_1}$) is inversely proportional to apparent strain. This value coupled with the shortening due to the initial buckling (figure B1.c) yields a value for total minimum shortening.

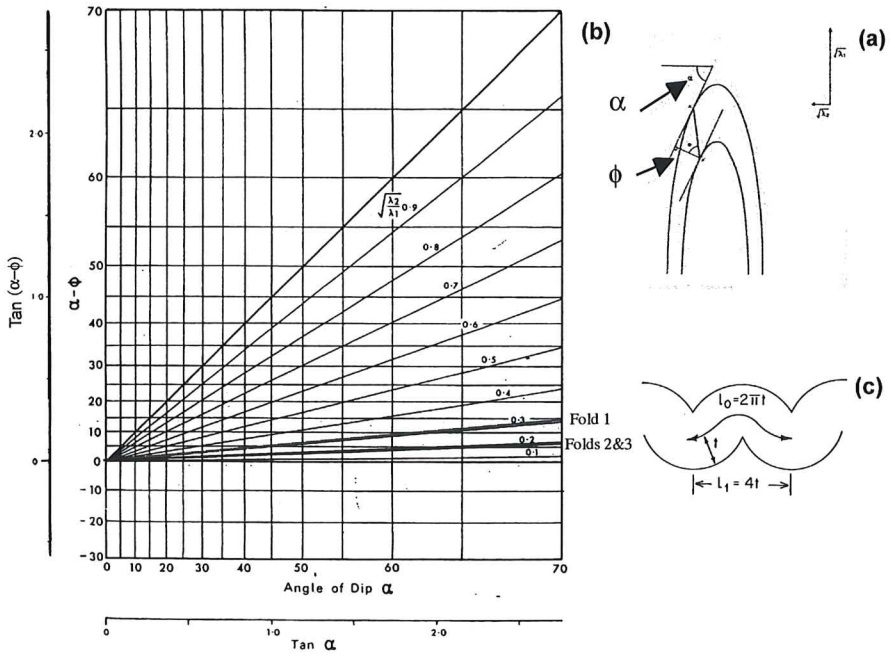

Figure B.1. (a) The relationship of the parameters α and ϕ as represented on a class 1(c) fold of Ramsey (1967). (b) Graphical plot of (α-ϕ) versus α and associated $\sqrt{\lambda_2}/\sqrt{\lambda_1}$ values for folds 1-3. (c) Parameters used to calculate initial buckling in class 1(b) folds.

Fold 1: sample no. A1121 – 11 (Plate 3a)

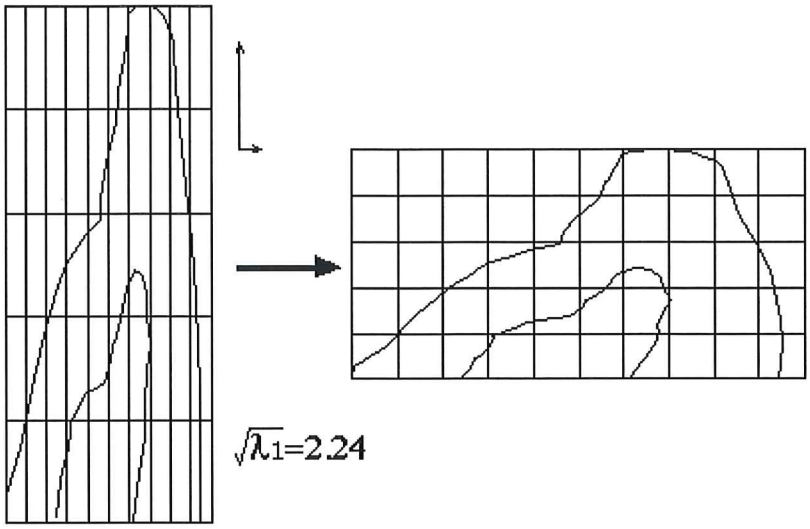

Shortening due to initial buckling:

$$L_0 = 117, L_1 = 73$$

$$\text{shortening} = \frac{L_0 - L_1}{L_0} \times 100$$

$$= \frac{117 - 73}{117} \times 100$$

$$= 60.3\%$$

Shortening due to flattening (Class 1b – 1c):

$$\sqrt{\lambda_2}/\sqrt{\lambda_1} = 0.2 \ (\alpha = 60, \phi = 56)$$

assuming original unit length:

$$\sqrt{\lambda_1} = \frac{\sqrt{1}}{\sqrt{0.2}} = 2.24$$

$$\therefore \sqrt{\lambda_2} = \sqrt{0.2}$$

$$= 0.45$$

$$\therefore \text{shortening} = \frac{1 - \sqrt{\lambda_2}}{1} \times 100$$

$$= \frac{1 - 0.45}{1} \times 100$$

$$= 55\%$$

$\therefore$ Total minimum shortening = 60.3 + 0.55(100 – 60.3)

=82.1%

Fold 2: sample no. A1121 – B (Plate 3b)

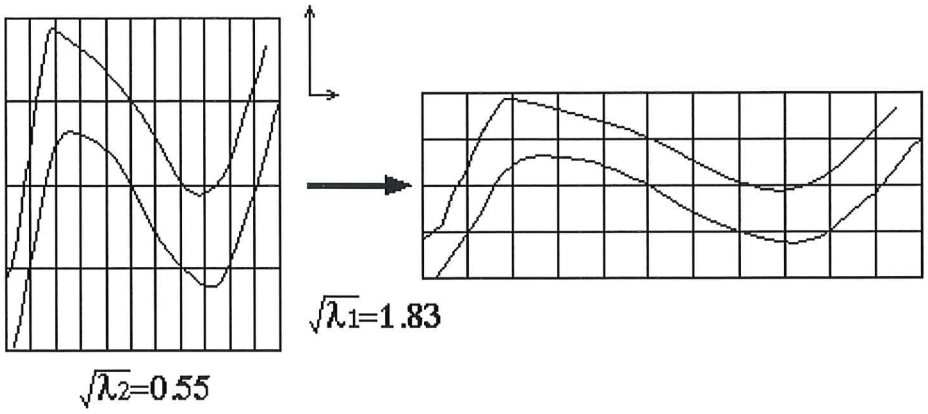

Shortening due to initial buckling:

$$L_0 = 66,\ L_1 = 58$$

$$\text{shortening} = \frac{L_0 - L_1}{L_0} \times 100$$

$$= \frac{66 - 58}{66} \times 100$$

$$= 12.1\%$$

Shortening due to flattening (Class 1b – 1c):

$\sqrt{\lambda_2}/\sqrt{\lambda_1} = 0.3$ ($\alpha = 65$, $\phi = 56$)

assuming original unit length:

$$\sqrt{\lambda_1} = \frac{\sqrt{1}}{\sqrt{0.3}} = 1.83$$

$$\therefore \sqrt{\lambda_2} = \sqrt{0.3}$$

$$= 0.55$$

$$\therefore \text{shortening} = \frac{1 - \sqrt{\lambda_2}}{1} \times 100$$

$$= \frac{1 - 0.55}{1} \times 100$$

$$= 45\%$$

$\therefore$ Total minimum shortening = 12.1 + 0.45(100 – 12.1)

=51.7%

Fold 3: sample no. A1121 – 13 (Plate 3c)

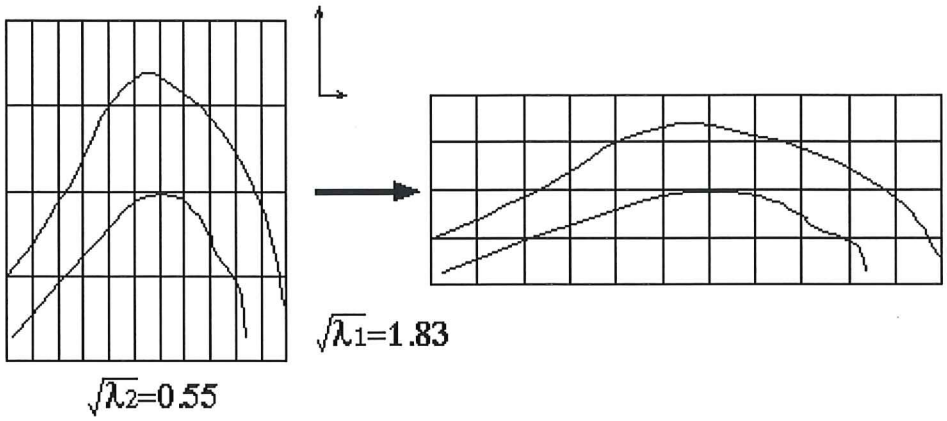

Shortening due to initial buckling:

$$L_0 = 98,\ L_1 = 87$$

$$\text{shortening} = \frac{L_0 - L_1}{L_0} \times 100$$

$$= \frac{98 - 87}{98} \times 100$$

$$= 11.2\%$$

Shortening due to flattening (Class 1b – 1c):

$$\sqrt{\lambda_2}/\sqrt{\lambda_1} = 0.3\ (\alpha = 65,\ \phi = 55)$$

assuming original unit length:

$$\sqrt{\lambda_1} = \frac{\sqrt{1}}{\sqrt{0.3}} = 1.83$$

$$\therefore \sqrt{\lambda_2} = \sqrt{0.3}$$

$$= 0.55$$

$$\therefore \text{shortening} = \frac{1 - \sqrt{\lambda_2}}{1} \times 100$$

$$= \frac{1 - 0.55}{1} \times 100$$

$$= 45\%$$

$\therefore$ Total minimum shortening = 11.2 + 0.45(100 – 11.2)

=51.2%

Rf/ϕ ANALYSIS

Dunnet (1969) initially proposed the Rf/ϕ method for determining the finite strains of deformed aggregates of initially non-spherical, sub-elliptical particles. Ramsey and Huber (1987) provide a step by step explanation for this method. An ellipse with initial ellipticity R_i, when homogenously deformed will take on the form of another ellipse R_f. The shape of this final ellipse is a function of the form and orientation of the strain ellipse. The method involves the calculation of the final deformed axial ratio (R_f) and the angle the long axis of this ellipse makes with the maximum principle strain direction (ϕ). The maximum principle strain direction was determined in each sample (hand specimen and thin section) as the principle foliation.

The finite strain axial ratio (R_s) and the initial undeformed particle axial ratio (R_i) can be determined using a series of experimentally derived graphs and the formulae given below. A computer program called INSTRAIN (Erslev, 1989) was used to calculate R_{fmax} and R_{fmin}. R_i and R_s were then calculated using the following formulae:

$$R_{fmax} = R_s \times R_i$$

$$R_{fmin} = \text{greater of} \left\{ \frac{R_s}{R_i} , \frac{R_i}{R_s} \right\}$$

The relative lengths of the X, Y and Z axes for the initial and final ellipse can also be calculated using the above formulae. The percentage shortening can be calculated using the formulae below. The intermediate axis of the strain ellipsoid (Y) needs to be normalised to 1, before this calculation is made.

$$\% \text{ shortening} = \frac{r - Z}{r} \times 100$$

$$\text{where } r = \sqrt[3]{X \times Y \times Z} \quad (Y = 1)$$

Sample no. A1121-3

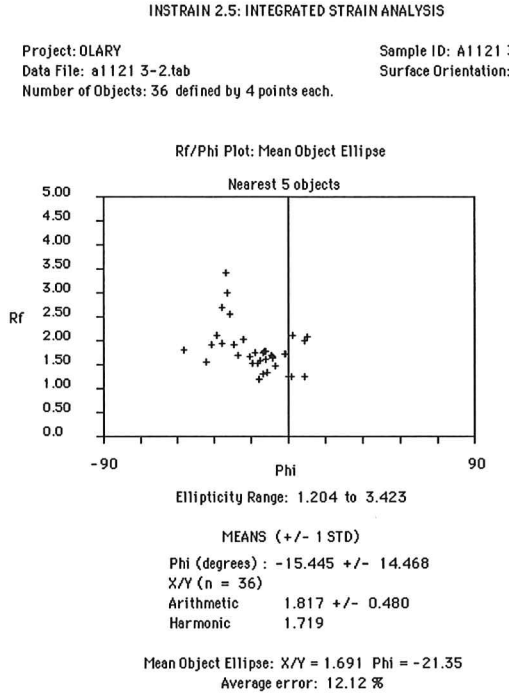

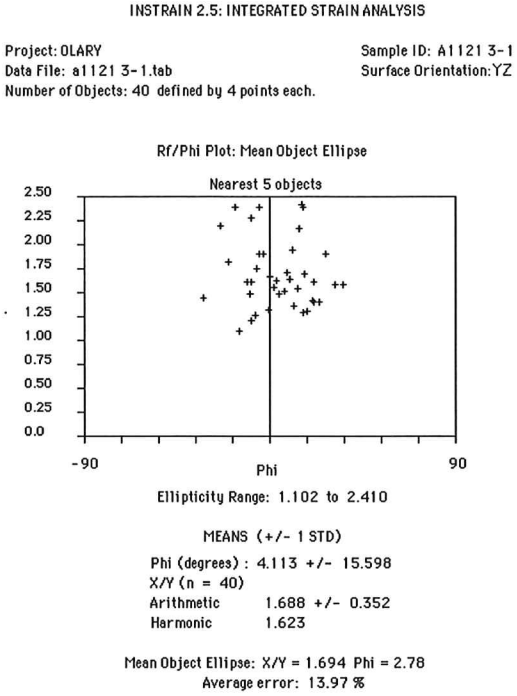

XZ section

$Rf_{min} = 1.204,\ Rf_{max} = 3.423$

$$\text{for } Rf_{min} = \frac{Rs}{Ri},\ \Rightarrow Rs = Rf_{min} \times Ri$$

$$\therefore Rf_{max} = Rf_{min} \times (Ri)^2$$

$$\Rightarrow Ri = \sqrt{\frac{Rf_{max}}{Rf_{min}}}$$

$$= 1.69$$

$$\Rightarrow Rs = \frac{Rf_{max}}{Ri}$$

$$= 2.03$$

YZ section

$Rf_{min} = 1.102,\ Rf_{max} = 2.410$

$$\text{for } Rf_{min} = \frac{Rs}{Ri},\ \Rightarrow Rs = Rf_{min} \times Ri$$

$$\therefore Rf_{max} = Rf_{min} \times (Ri)^2$$

$$\Rightarrow Ri = \sqrt{\frac{Rf_{max}}{Rf_{min}}}$$

$$= 1.48$$

$$\Rightarrow Rs = \frac{Rf_{max}}{Ri}$$

$$= 1.63$$

$\therefore$ Ri (X:Y:Z) = (1.69:1.48:1.0), Rs (X:Y:Z) = (2.03:1.63:1.0)

$$\% \text{ shortening} = \frac{r - Z}{r} \times 100$$

$$= \frac{0.91 - 0.61}{0.91} \times 100$$

$$= 33.0\%$$

Sample no. A1121-6

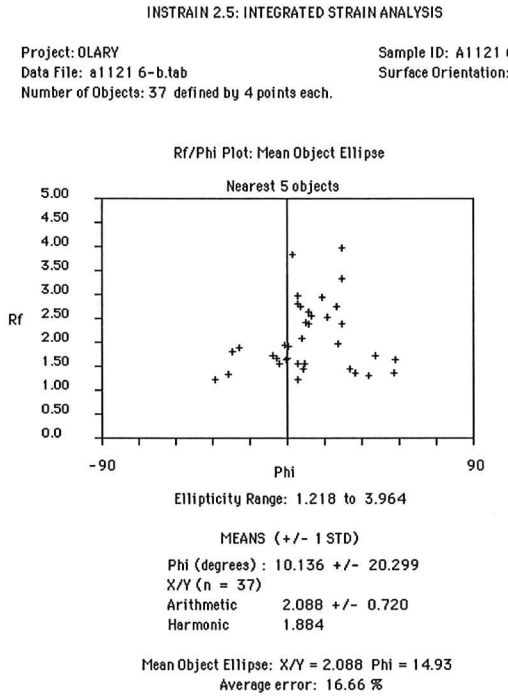

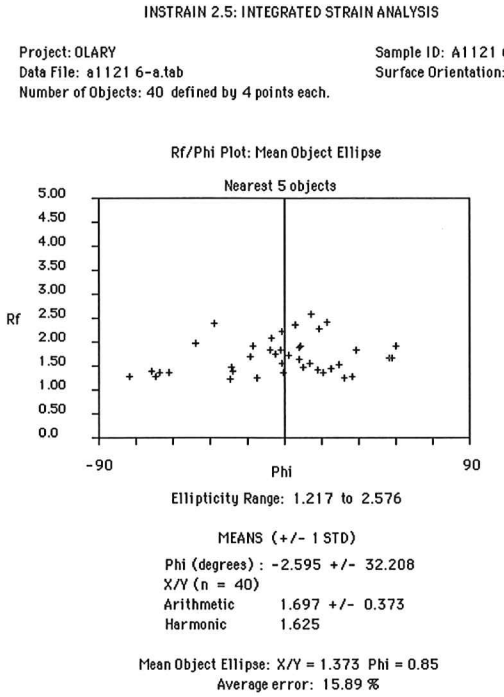

XZ section

$Rf_{min} = 1.218,\ Rf_{max} = 3.964$

$$\text{for } Rf_{min} = \frac{Rs}{Ri},\ \Rightarrow Rs = Rf_{min} \times Ri$$

$$\therefore Rf_{max} = Rf_{min} \times (Ri)^2$$

$$\Rightarrow Ri = \sqrt{\frac{Rf_{max}}{Rf_{min}}}$$

$$= 1.804$$

$$\Rightarrow Rs = \frac{Rf_{max}}{Ri}$$

$$= 2.197$$

YZ section

$Rf_{min} = 1.217,\ Rf_{max} = 2.576$

$$\text{for } Rf_{min} = \frac{Rs}{Ri},\ \Rightarrow Rs = Rf_{min} \times Ri$$

$$\therefore Rf_{max} = Rf_{min} \times (Ri)^2$$

$$\Rightarrow Ri = \sqrt{\frac{Rf_{max}}{Rf_{min}}}$$

$$= 1.455$$

$$\Rightarrow Rs = \frac{Rf_{max}}{Ri}$$

$$= 1.77$$

$\therefore$ Ri (X:Y:Z) = (1.80:1.46:1.0), Rs (X:Y:Z) = (2.20:1.77:1.0)

$$\% \text{ shortening} = \frac{r - Z}{r} \times 100$$

$$= \frac{0.92 - 0.59}{0.92} \times 100$$

$$= 35.9\%$$

Sample no. A1121-10

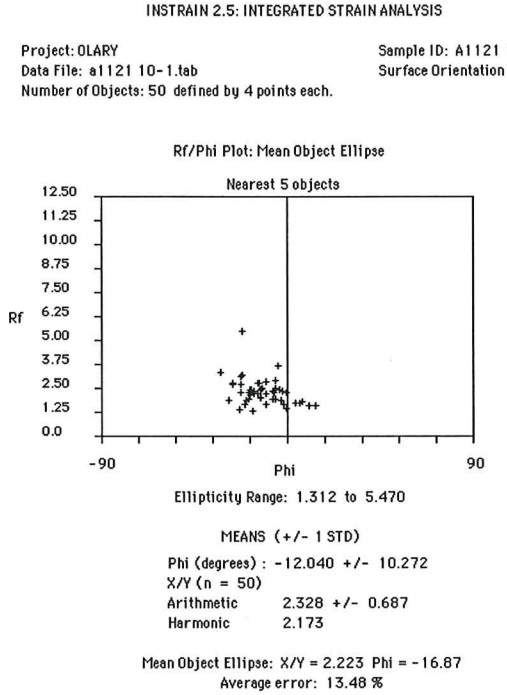

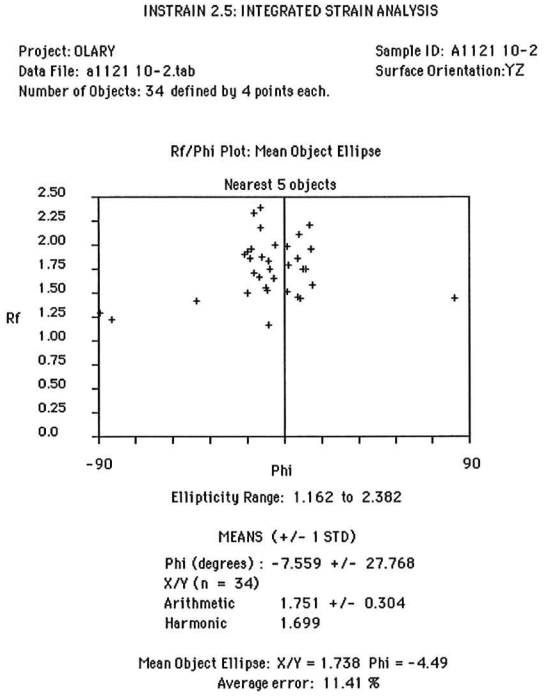

XZ section

$$Rf_{min} = 1.312,\ Rf_{max} = 5.470$$

$$\text{for } Rf_{min} = \frac{Rs}{Ri},\ \Rightarrow Rs = Rf_{min} \times Ri$$

$$\therefore Rf_{max} = Rf_{min} \times (Ri)^2$$

$$\Rightarrow Ri = \sqrt{\frac{Rf_{max}}{Rf_{min}}}$$

$$= 2.04$$

$$\Rightarrow Rs = \frac{Rf_{max}}{Ri}$$

$$= 2.68$$

YZ section

$$Rf_{min} = 1.162,\ Rf_{max} = 2.382$$

$$\text{for } Rf_{min} = \frac{Rs}{Ri},\ \Rightarrow Rs = Rf_{min} \times Ri$$

$$\therefore Rf_{max} = Rf_{min} \times (Ri)^2$$

$$\Rightarrow Ri = \sqrt{\frac{Rf_{max}}{Rf_{min}}}$$

$$= 1.43$$

$$\Rightarrow Rs = \frac{Rf_{max}}{Ri}$$

$$= 1.67$$

$$\therefore Ri\ (X:Y:Z) = (2.04:1.43:1.0),\ Rs\ (X:Y:Z) = (2.68:1.67:1.0)$$

$$\%\ \text{shortening} = \frac{r - Z}{r} \times 100$$

$$= \frac{0.99 - 0.6}{0.99} \times 100$$

$$= 39.4\%$$

Sample no. A1121-12

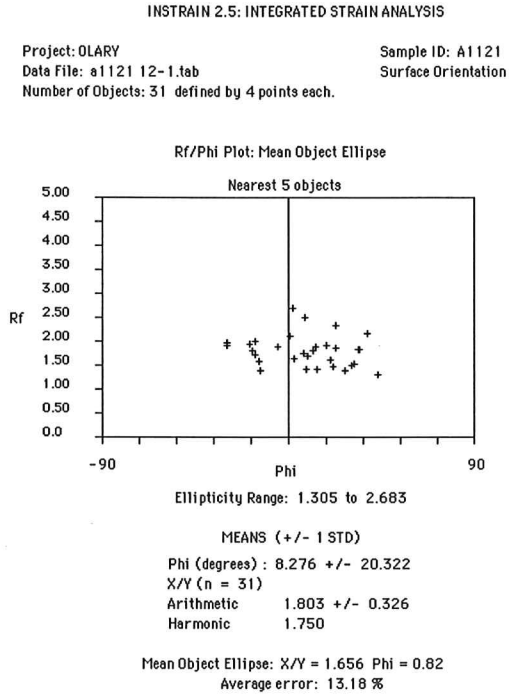

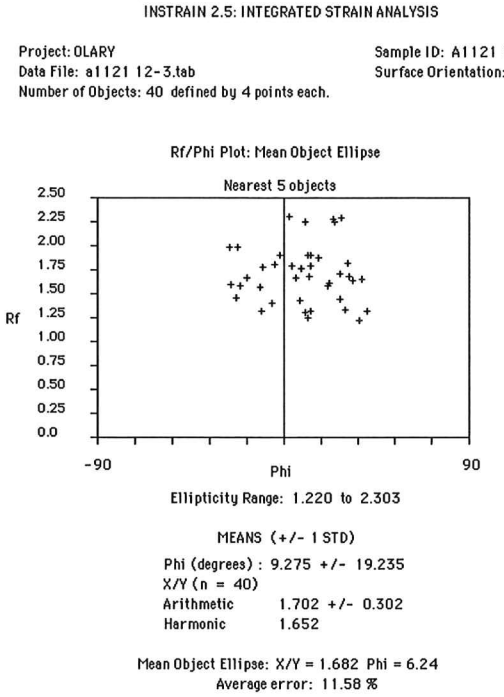

XZ section

$$Rf_{min} = 1.305,\ Rf_{max} = 2.683$$

$$\text{for } Rf_{min} = \frac{Rs}{Ri},\ \Rightarrow Rs = Rf_{min} \times Ri$$

$$\therefore Rf_{max} = Rf_{min} \times (Ri)^2$$

$$\Rightarrow Ri = \sqrt{\frac{Rf_{max}}{Rf_{min}}}$$

$$= 1.43$$

$$\Rightarrow Rs = \frac{Rf_{max}}{Ri}$$

$$= 1.88$$

YZ section

$$Rf_{min} = 1.22,\ Rf_{max} = 2.303$$

$$\text{for } Rf_{min} = \frac{Rs}{Ri},\ \Rightarrow Rs = Rf_{min} \times Ri$$

$$\therefore Rf_{max} = Rf_{min} \times (Ri)^2$$

$$\Rightarrow Ri = \sqrt{\frac{Rf_{max}}{Rf_{min}}}$$

$$= 1.37$$

$$\Rightarrow Rs = \frac{Rf_{max}}{Ri}$$

$$= 1.68$$

$$\therefore Ri\ (X:Y:Z) = (1.43:1.37:1.0),\ Rs\ (X:Y:Z) = (1.88:1.68:1.0)$$

$$\%\ \text{shortening} = \frac{r - Z}{r} \times 100$$

$$= \frac{0.88 - 0.6}{0.88} \times 100$$

$$= 31.8\%$$

Sample no. A1121-16

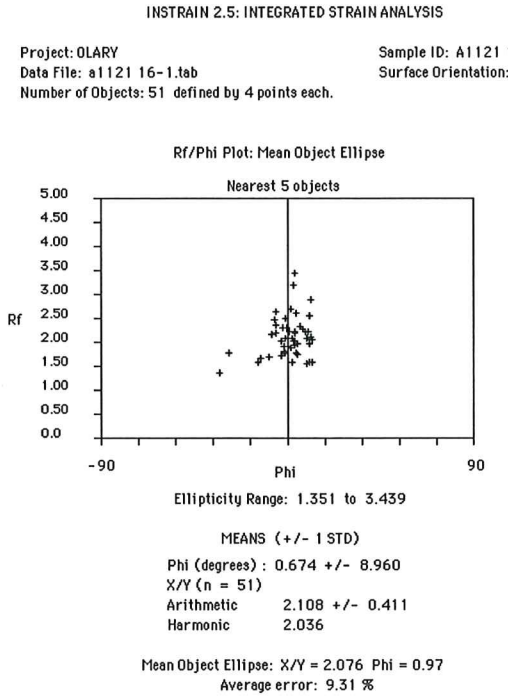

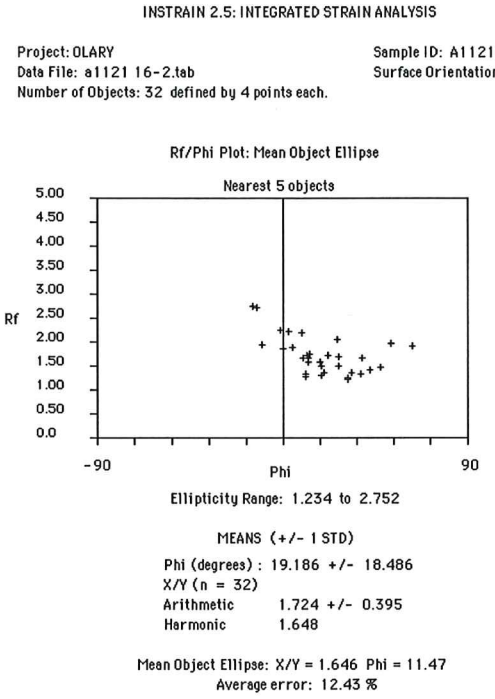

XZ section

$$Rf_{min} = 1.351,\ Rf_{max} = 3.439$$

$$\text{for } Rf_{min} = \frac{Rs}{Ri},\ \Rightarrow Rs = Rf_{min} \times Ri$$

$$\therefore Rf_{max} = Rf_{min} \times (Ri)^2$$

$$\Rightarrow Ri = \sqrt{\frac{Rf_{max}}{Rf_{min}}}$$

$$= 1.60$$

$$\Rightarrow Rs = \frac{Rf_{max}}{Ri}$$

$$= 2.15$$

YZ section

$$Rf_{min} = 1.234,\ Rf_{max} = 2.752$$

$$\text{for } Rf_{min} = \frac{Rs}{Ri},\ \Rightarrow Rs = Rf_{min} \times Ri$$

$$\therefore Rf_{max} = Rf_{min} \times (Ri)^2$$

$$\Rightarrow Ri = \sqrt{\frac{Rf_{max}}{Rf_{min}}}$$

$$= 1.49$$

$$\Rightarrow Rs = \frac{Rf_{max}}{Ri}$$

$$= 1.85$$

$$\therefore Ri\ (X:Y:Z) = (1.60:1.49:1.0),\ Rs\ (X:Y:Z) = (2.15:1.85:1.0)$$

$$\%\ \text{shortening} = \frac{r - Z}{r} \times 100$$

$$= \frac{0.86 - 0.54}{0.86} \times 100$$

$$= 37.2\%$$

Sample no. A1121-G

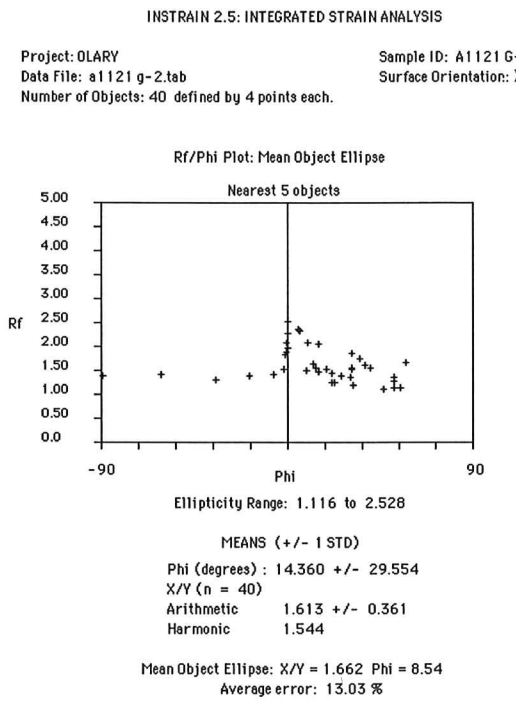

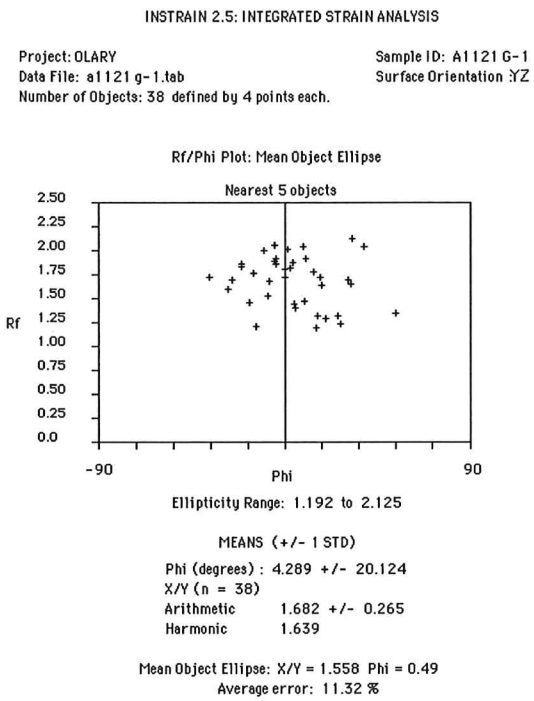

XZ section

$$Rf_{min} = 1.116,\ Rf_{max} = 2.528$$

$$\text{for } Rf_{min} = \frac{Rs}{Ri},\ \Rightarrow Rs = Rf_{min} \times Ri$$

$$\therefore Rf_{max} = Rf_{min} \times (Ri)^2$$

$$\Rightarrow Ri = \sqrt{\frac{Rf_{max}}{Rf_{min}}}$$

$$= 1.505$$

$$\Rightarrow Rs = \frac{Rf_{max}}{Ri}$$

$$= 1.680$$

YZ section

$$Rf_{min} = 1.192,\ Rf_{max} = 2.125$$

$$\text{for } Rf_{min} = \frac{Rs}{Ri},\ \Rightarrow Rs = Rf_{min} \times Ri$$

$$\therefore Rf_{max} = Rf_{min} \times (Ri)^2$$

$$\Rightarrow Ri = \sqrt{\frac{Rf_{max}}{Rf_{min}}}$$

$$= 1.335$$

$$\Rightarrow Rs = \frac{Rf_{max}}{Ri}$$

$$= 1.592$$

$$\therefore Ri\ (X:Y:Z) = (1.51:1.34:1.0),\ Rs\ (X:Y:Z) = (1.68:1.59:1.0)$$

$$\%\ \text{shortening} = \frac{r - Z}{r} \times 100$$

$$= \frac{0.87 - 0.63}{0.87} \times 100$$

$$= 27.6\%$$

δ - ANGLE ANALYSIS

Tables B.1 and B.2 list the structural data used to calculate the δ - angles discussed in chapter 6.

Sub area	Layering (So)		Schistosity (Sx)		Intersection lineation (lx)		Delta angle (d)
	dip	dip direction	dip	dip direction	dip	dip direction	
A	67	111	53	130	39.6	091.4	20.88
	88	200	89	186	77.9	100.7	14.32
	75	160	79	163	35.1	080.8	4.95
B	65	122	75	030	61.2	090.9	86.36
	77	161	80	175	73.1	120.5	14.04
	77	153	70	167	58.1	221.2	15.13
	85	160	84	172	82.7	207	11.99
	88	170	78	160	44.2	081.9	14.08
	78	160	83	172	65.2	097.4	12.84
	78	154	71	165	53.4	227.4	12.69
	78	154	71	166	55.4	226	13.51
	65	151	77	170	51.5	096.9	21.56
C	71	177	62	190	46.8	245.5	14.92
	71	136	65	156	61.5	006.5	19.47
	65	150	76	168	52	096.6	20.18
	60	138	80	150	27.1	065.2	22.92
	59	140	71	153	39.1	079.3	16.79
	66	139	68	156	65.7	129.5	15.77
	60	168	70	150	50.2	214.1	19.09
	85	319	82	130	34.5	045.5	15.8
	86	319	90	149	68.1	239	10.76
	77	153	70	167	58.1	221.2	15.13
	71	157	73	169	69.4	133.5	11.58
	71	177	62	190	46.8	245.5	14.92
	73	148	73	152	73.0	150	3.83
	85	123	82	135	74.4	194.7	12.29
	73	037	74	048	72.6	114.1	10.59
	74	038	75	047	73.1	109.2	8.73
	75	036	80	047	62.2	066.5	11.84

Table B.1: Structural Data used to determine δ - angles in sub areas A-C.

Sub area	Layering (So)		Schistosity (Sx)		Intersection lineation (lx)		Delta angle (d)
	dip	dip direction	dip	dip direction	dip	dip direction	
D	77	156	85	171	60.2	089.8	16.82
	73	165	60	143	49.9	096.3	22.93
	69	153	68	163	67.6	354.3	9.36
	78	132	79	144	77.5	295	11.8
	69	144	78	166	61.5	279.1	22.9
	68	127	84	121	19.2	208.9	17.02
	70	126	75	140	63.1	261.9	14.25
	83	118	80	131	74.3	002	13.2
	76	138	75	153	74.9	340	14.55
	73	113	77	127	67.7	251	14.1
	80	146	80	149	80	324.5	8.86
	74	145	77	155	67.6	279	10.13
	64	140	57	150	42.6	023.4	11.16
	73	176	73	159	72.8	167.5	16.25
	65	205	69	188	62.9	229.5	16.14
	82	146	85	154	68.3	256.7	8.49
	69	131	64	148	60.6	358.1	16.36
	80	134	73	146	55.4	028.6	13.6
	90	140	73	149	77.1	050	19.17
	68	129	87	169	60.4	264.3	43.21
	71	140	83	025	65.6	099.3	69.09
	77	097	82	131	76.1	255.5	33.77

Table B.2: Structural Data used to determine δ - angles in sub area D.